Progress in Neuropsychopharmacology & Biological Psychiatry 136 (2025) 111167

Contents lists available at ScienceDirect

Progress in Neuropsychopharmacology & Biological Psychiatry

journal homepage: www.elsevier.com/locate/pnp

Involvement of muscarinic acetylcholine receptor-mediated cholinergic neurotransmission in TMS–EEG responses

Yufei Song [a,b], Pedro C. Gordon [a,b], Olivier Roy [a,b,c,d], Johanna Metsomaa [e], Paolo Belardinelli [a,b,f], Maryam Rostami [g], Ulf Ziemann [a,b,*]

[a] Department of Neurology & Stroke, University of Tübingen, Germany
[b] Hertie Institute for Clinical Brain Research, University of Tübingen, Germany
[c] CERVO Brain Research Centre, Quebec, Canada
[d] Department of Psychiatry and Neurosciences, Université Laval, Quebec, Canada
[e] Department of Neuroscience and Biomedical Engineering, Aalto University School of Science, Finland
[f] CIMeC, Center for Mind/Brain Sciences, University of Trento, Italy
[g] Faculty of Electrical and Computer Engineering, University of Tehran, Iran

ARTICLE INFO

Keywords:
Transcranial magnetic stimulation-electroencephalography
Pharmacological TMS–EEG
mAChR
Evoked-potentials
Oscillations

ABSTRACT

The combination of transcranial magnetic stimulation and electroencephalography (TMS–EEG) is emerging as a valuable tool for investigating brain functions in health and disease. However, the detailed neural mechanisms underlying TMS–EEG responses, including TMS-evoked EEG potentials (TEPs) and TMS-induced EEG oscillations (TIOs), remain largely unknown. Combining TMS–EEG with pharmacological interventions provides a unique opportunity to elucidate the roles of specific receptor-mediated neurotransmissions in these responses. Here, we investigated the involvement of muscarinic acetylcholine receptor (mAChR)-mediated cholinergic neurotransmission in TMS–EEG responses by evaluating the effects of mAChR antagonists on TEPs and TIOs in twenty-four healthy participants using a randomized, placebo-controlled crossover design. TEPs and TIOs were measured before and after administering a single oral dose of scopolamine (a non-selective mAChR antagonist), biperiden (an M1 mAChR antagonist), or placebo, with TMS targeting the left medial prefrontal cortex (mPFC), angular gyrus (AG), and supplementary motor area (SMA). The results indicated that mAChR-mediated cholinergic neurotransmission played a role in TEPs, but not TIOs, in a target-specific manner. Specifically, scopolamine significantly increased the amplitude of a local TEP component between approximately 40 and 63 ms post-stimulus when TMS was applied to the SMA, but not the mPFC or AG. Biperiden produced a similar but less pronounced effect. Importantly, the effects of these mAChR antagonists on TEPs were independent of those on sensory-evoked EEG potentials caused by TMS-associated sensory stimulation. These findings expand our understanding of TMS–EEG physiology, providing insights for its application in physiological and clinical research.

1. Introduction

Transcranial magnetic stimulation coupled with electroencephalography (TMS–EEG) is an effective, non-invasive tool for investigating brain functions, such as excitability and connectivity (Ilmoniemi et al., 1997). Two commonly used outcome measures in TMS–EEG studies are TMS-evoked EEG potentials (TEPs) and TMS-induced EEG oscillations (TIOs). Both measures are time-locked responses to direct cortical activation elicited by single-pulse TMS targeting specific brain regions. TEPs capture phase-locked brain activity and are typically analyzed in the time domain, revealing a sequence of positive (P) and negative (N) peaks sensitive to stimulation parameters such as site and intensity (Cohen, 2014; Hernandez-Pavon et al., 2023). In contrast, TIOs are often assessed using time-frequency decomposition techniques, enabling the extraction of non-phase-locked oscillatory power (Belardinelli et al., 2021; Gordon et al., 2021; Pellicciari et al., 2017; Premoli et al., 2017). A typical time-frequency representation (TFR) of TIOs shows synchronization (power increase) and desynchronization (power decrease) as functions of frequency and time. Changes in these TMS–EEG measures have been described in various neurological and psychiatric disorders compared to healthy controls, highlighting their potential as biomarkers for diagnosis and treatment monitoring (reviewed in (Tremblay et al.,

* Corresponding author at: Department of Neurology & Stroke, Hoppe-Seyler-Straße 3, 72076 Tübingen, Germany.
E-mail address: ulf.ziemann@uni-tuebingen.de (U. Ziemann).

https://doi.org/10.1016/j.pnpbp.2024.111167
Received 24 June 2024; Received in revised form 1 October 2024; Accepted 3 October 2024
Available online 9 October 2024

2019)). However, translating TMS–EEG measures into clinical practice requires a deeper understanding of their physiological underpinnings.

TMS induces action potentials by depolarizing axons of a mixed neural population in the stimulated cortex (Hernandez-Pavon et al., 2023; Siebner et al., 2022). The initial current travels along axons, producing local excitation or inhibition within the targeted area as well as remote effects on interconnected cortical and subcortical regions. The synchrony of postsynaptic potentials generated along this route results in measurable EEG signals (Jackson and Bolger, 2014). This chain of electrical activity is mediated through neurotransmitter-mediated processes. Glutamate and GABA are the primary excitatory and inhibitory neurotransmitters in the brain, respectively. Recent pharmacological TMS–EEG studies have demonstrated the involvement of GABAergic and glutamatergic neurotransmission in TMS–EEG responses in healthy participants (Belardinelli et al., 2021; Cash et al., 2017; Darmani et al., 2016; Gordon et al., 2023b; Hui et al., 2020; Premoli et al., 2014, 2017; Salavati et al., 2018). The intake of diazepam (a GABAA receptor positive allosteric modulator) increased the amplitude of the N45 TEP and decreased the amplitude of the P60, N100, and P150 TEP when applying single-pulse TMS to the primary motor cortex (M1) (Gordon et al., 2023b; Premoli et al., 2014). Diazepam also enhanced the TMS-induced EEG alpha power and, conversely, suppressed beta power (Gordon et al., 2023b; Premoli et al., 2017). Moreover, the intake of the anti-glutamatergic drug dextromethorphan (an NMDA receptor antagonist) also increased N45 amplitude, with a similar EEG topology as diazepam (Belardinelli et al., 2021). In contrast, the alpha5-GABAA receptor antagonist compound S44819 decreased N45 amplitude (Darmani et al., 2016). This body of evidence suggests TMS–EEG responses reflect the balance of excitatory and inhibitory neurotransmission. In addition, neuromodulators like acetylcholine (ACh) and dopamine regulate the excitatory and inhibitory transmission initiated by glutamate and GABA in neural circuits (Nadim and Bucher, 2014; Tsuboi et al., 2024). However, the involvement of neuromodulator-mediated neurotransmission in TMS–EEG responses remains largely unexplored.

ACh plays a crucial role in modulating cognitive (Bentley et al., 2011) and motor (Maurice et al., 2015) functions. Deficits in ACh-mediated cholinergic signaling have been implicated in neurodegenerative diseases, such as Alzheimer's disease (AD), Lewy body dementia, and Parkinson's disease (PD) (Bohnen et al., 2018). Therefore, exploring the involvement of cholinergic neurotransmission in TMS–EEG responses is potentially clinically valuable. If TEPs and TIOs are sensitive to the manipulation of cholinergic signaling, they may serve as non-invasive indicators of cholinergic system (dys)function. In the brain, ACh is primarily released from cholinergic projection neurons in the basal forebrain nuclei (BF), the brainstem, and local cholinergic interneurons in the striatum (Ballinger et al., 2016; Picciotto et al., 2012; Thiele, 2013). ACh acts on muscarinic ACh receptors (mAChRs) and nicotinic receptors (nAChRs). mAChRs are metabotropic G-protein coupled receptors with five subtypes (M1–M5), with M1-M4 receptors being abundant in both the cortex and striatum. At the cellular level, presynaptic M2 and M4 receptors act as inhibitory autoreceptors on cholinergic terminals and heteroreceptors on GABAergic and glutamatergic terminals, suppressing neurotransmitter release (Colangelo et al., 2019; Thiele, 2013). Conversely, postsynaptic M1 and M3 receptors, expressed on both interneurons and pyramidal cells, influence neuronal excitability by modulating ion channels. Consequently, mAChR-mediated neurotransmission finely tunes the information flow by influencing neuronal excitability and synaptic efficacy. Similar to mAChRs, nAChRs have multiple subtypes and are expressed in diverse neural populations. Though nAChRs function as excitatory cation channels, the activation of nAChRs in the brain is largely modulatory as well.

In this study, we investigated whether and how TEPs and TIOs are affected by the inhibition of cholinergic neurotransmission. nAChR antagonists are not commonly used in healthy populations due to the transient paralysis caused by blocking nicotinic activity at the neuromuscular junction (Kunnath et al., 2023). Therefore, we employed two mAChR antagonists, scopolamine and biperiden, to inhibit muscarinic cholinergic transmission. Scopolamine is a non-selective receptor antagonist, while biperiden selectively blocks the M1 receptor (Bakker et al., 2021; Klinkenberg and Blokland, 2010). For TMS targets, we chose the left medial prefrontal cortex (mPFC), angular gyrus (AG), and supplementary motor area (SMA). The mPFC and AG are integral to brain networks critical for cognitive functions, where the cholinergic system plays an important role (Bentley et al., 2011; Klinkenberg et al., 2011). The SMA is involved in motor control, which is regulated by neuromodulatory systems including cholinergic signaling (Maurice et al., 2015). We conducted a randomized, placebo-controlled crossover study in which healthy participants received a single oral dose of scopolamine (SCO), biperiden (BIP), or placebo (PLA) in three separate sessions. During each session, we measured TEPs and TIOs in response to TMS of the three brain regions before and after drug administration. We hypothesized that scopolamine and biperiden, but not placebo, would significantly alter TEPs and TIOs. Additionally, we anticipated differential effects between scopolamine and biperiden due to their receptor selectivity.

2. Methods

2.1. Participants

The study was approved by the ethics committee of the medical faculty of Tübingen University (protocol number 638/2020BO1) and was conducted in accordance with the Declaration of Helsinki. All participants provided written informed consent prior to the inclusion in the study. The inclusion criteria required that participants had no prior history of illnesses such as cardiovascular, hepatic, renal, pulmonary, gastrointestinal, neurological, or psychiatric disorders, nor were they taking any medication with effects on the central nervous system (CNS). All participants underwent a medical screening to check for any contraindications to TMS and study drugs, including a 12-lead electrocardiogram (ECG). Twenty-eight healthy participants (mean age ± SD, 26.0 ± 4.8 years; 16 females) were included in the study, and twenty-four participants (mean age ± SD, 25.7 ± 4.8 years; 14 females) completed all the sessions: three participants dropped out, and one participant did not comply with the experimenting procedures. Therefore, the final analysis was based on twenty-four participants.

2.2. Experimental design and procedure

We conducted a placebo-controlled cross-over study, which involved three experimental sessions per participant, each separated by at least one week (Fig. 1). During each session, participants were administered a single oral dose of either scopolamine (0.9 mg, Kwells®, Dexcel® pharma GmbH), biperiden (4 mg, Akineton®, Desma GmbH), or placebo (PTabletten 8 mm Lichtenstein, Zentiva Pharma GmbH). The drug order was randomized and balanced over the three sessions across participants. Each session included three blocks of TMS–EEG recordings targeting the mPFC, AG, and SMA, respectively. This was followed by a simple reaction time (SRT) task. These measurements were repeated 60 min after drug intake. To control for TMS-associated sensory inputs, a sham procedure was used during TMS–EEG recordings, involving both *active* TMS and *sham* TMS conditions (Methods: Section 2.3).

2.3. TMS–EEG setup

TMS–EEG recordings contain EEG responses to TMS-associated peripheral sensory inputs (somatosensory and auditory), which can introduce ambiguity when interpreting results in pharmacological TMS–EEG studies. This ambiguity arises because CNS-active drugs may alter not only the genuine TMS–EEG responses resulting from direct cortical activation elicited by TMS but also the EEG responses caused by

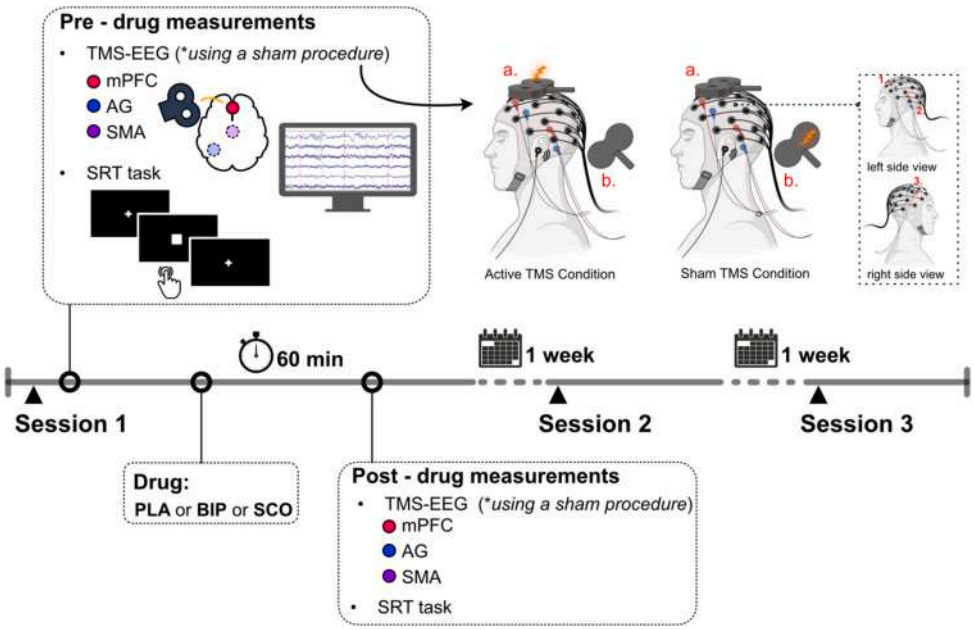

Fig. 1. Study timeline. This randomized, placebo-controlled cross-over study consisted of three sessions (PLA, BIP, SCO), each separated by one week. Each session included three blocks of TMS-EEG recordings targeting the mPFC, AG, and SMA, followed by a SRT task. Measurements were repeated 60 min after drug intake. To control for TMS-associated sensory inputs, a sham procedure was used, involving both active TMS and sham TMS conditions. The upper panel shows the experimental setup for targeting the SMA (adapted with permission from Song et al., 2023). Two identical TMS coils (a and b) were used: Coil a delivered TMS pulses to the SMA in the active condition, while Coil b produced the 'click' sound in the sham condition. ES pulses were delivered concomitantly with TMS pulses via three pairs of bipolar electrodes in both conditions. Masking noise was played throughout the recording. Abbreviations: AG: angular gyrus; BIP, biperiden; ES: electrical stimulation; mPFC: medial prefrontal cortex; PLA, placebo; SCO, scopolamine; SMA, supplementary motor area; SRT: simple reaction time; TMS-EEG, Transcranial magnetic stimulation-Electroencephalography.

sensory inputs (Gordon et al., 2023b). Consequently, it becomes challenging to determine to what extent observed changes in TMS–EEG signals following the drug administration are due to drug effects on direct cortical activation or sensory processing. A common approach to address these sensory confounds is to include a sham stimulation that replicates TMS-associated sensory inputs. Several studies have attempted to mimic TMS-associated auditory inputs with TMS 'click' generated by a TMS coil placed at an angle or a distance from the head and recreate somatosensory inputs using scalp electrical stimulation (ES) (Chowdhury et al., 2022; Conde et al., 2019; Fernandez et al., 2021). However, due to the distinct biophysical mechanisms involved in ES and TMS, precisely matching sensory-related EEG responses between sham and active conditions remains challenging (Conde et al., 2019). To mitigate this, we employed a sham procedure developed and validated in our previous work, which involves applying high-intensity ES to both *sham* and *active* TMS conditions (Gordon et al., 2021, 2023a). This approach aims to saturate the EEG response to sensory inputs, thereby minimizing the impact of any additional somatosensory inputs caused by TMS in the active condition. As a result, the sensory components between the two conditions become closely matched, allowing for reliable subtraction of *sham* EEG from the *active* condition and facilitating the identification of direct cortical activation by TMS.

Fig. 1 illustrates an example of applying TMS to the SMA. In the *active* TMS condition, a TMS stimulator (Magstim® 200^2, monophasic mode, UK) equipped with a figure-of-eight coil (external diameter = 90 mm) was used. To estimate and monitor coil positions during TMS–EEG recordings, we used a navigation system (TMS Navigator, Localite GmbH, Germany). Magnetic resonance imaging (MRI) with a T1-weighted anatomical sequence for each participant was recorded prior to TMS–EEG sessions. We aligned the individual T1w image with the Talairach coordinate system. The cortical targets were defined by the Montreal Neurological Institute (MNI) coordinates (left mPFC: −4, 52, 36; left AG: −42, −69, 31; left SMA: −2, −7, 55). Aiming to target the desired cortical locations, we positioned the *active* TMS coil perpendicular to the underlying gyrus. The induced current ran approximately from lateral to medial for targeting the mPFC and SMA and from posterior-medial to anterior-lateral for targeting the AG. The intensity in the *active* TMS condition was set to 120 % resting motor threshold (RMT). To determine the RMT, we attached bipolar surface electromyographic (EMG) electrodes to the abductor pollicis brevis (APB), and first dorsal interosseus (FDI) muscles of the participant's right hand, EMG signals were sampled at 5 kHz (device filter DC-1250 Hz). We targeted the hotspot of M1, defining RMT as the lowest intensity that produced an MEP over 50 μV in at least 5 out of 10 consecutive pulses (Groppa et al., 2012). In the *sham* TMS condition, to generate the TMS associated 'click' sound, we used a second TMS setup identical to the one in the *active* TMS condition. The second TMS coil was placed near the participant's head, with the intensity set to 1.6 x *active* TMS to account for the increased distance (Gordon et al., 2021). To mimic TMS-associated somatosensory inputs, we delivered ES pulses (Digitimer DS7A, Digitimer Ltd.UK) through short-distance bipolar electrodes attached to the EEG cap with the following montage: pair 1 (frontal: AFF1H, AFF5H) and pair 2 (parietal: TPP7H, TPP9H) in the left hemisphere, and pair 3 (central: FFC4H, FCC4H) in the right hemisphere. These positions were chosen to be near the three TMS sites, respectively. To closely approximate sensory-related EEG responses in both *sham* TMS and *active* TMS conditions, we aimed to saturate the EEG response to sensory inputs. This was done by delivering ES pluses to both *sham* and *active* conditions using a high intensity of 24 mA (width 200 μs, maximum voltage of 400 V) through the three pairs of electrodes. ES pulses were concomitant with TMS pulses, and the three pairs of electrodes were fired together. The current polarity was switched after each pulse. Additionally, masking noise was played throughout the recording for both *sham* and *active* TMS conditions (Massimini et al., 2005).

2.4. TMS–EEG data recording

EEG signals were recorded with a TMS-compatible system (NeurOne,

Bittium, Kuopio, Finland). 64 Ag/AgCl sintered ring electrodes were placed according to the International 10–5 system in an elastic cap (EasyCap BC-TMS-64, EasyCap, Germany). We used electrode CPz as the online reference and placed the ground at PPO1h. EEG signals were sampled at 5 kHz (device filter DC-1250 Hz), and EEG electrode impedances were maintained below 5 kΩ. We digitized the electrodes' positions from the navigation system for source reconstruction purposes. We recorded 150 *active* TMS pulses and 50 *sham* TMS pulses in each TMS–EEG block, with the *sham* TMS pulses randomly interleaved within the *active* TMS pulses. This resulted in a total of 150 pulses for the *sham* conditions across the three TMS–EEG blocks. The ISI was 3 s (±1 s jitter; 2–4 s range).

2.5. TMS–EEG data preprocessing

Offline EEG preprocessing and analysis were performed in a Matlab environment (version 2022b, MathWorks Inc.). EEGLAB (Delorme and Makeig, 2004), FieldTrip (Oostenveld et al., 2011), and customized scripts were used. We employed the preprocessing pipeline established in our previous work (Metsomaa et al., 2024; Song et al., 2023). The TMS–EEG signals were preprocessed individually, one TMS site at a time. We first epoched the continuous signal into 3000 ms trials (−1500 to 1500 ms around stimuli) and corrected the baseline with respect to the −1000 to −5 ms pre-stimulus time window. We next grouped *sham* and *active* TMS trials, as well as pre- and post-drug conditions from the same session, to ensure consistent artifact rejection along the pipeline. Following a robust detrending (3rd-order polynomial fitting), we re-epoched the data into shorter trials (−1000 to 1000 ms). Decay artifacts were removed with a customized function (Supplementary Materials: Section 1.1) on a trial-by-trial basis. Subsequently, pulse artifacts (−4 to 17 ms) were eliminated and cubic-interpolated. We then resampled to 1 kHz ('resample' function in Matlab, including low-pass filtering at the Nyquist frequency). Channels and trials heavily contaminated by noise or artifacts were manually excluded. We next applied FastICA to identify ocular artifact topographies, which were removed using a beamforming filter in a later step. The SSP–SOUND joint algorithm was employed to estimate the signal subspace containing TMS-related artifacts and suppress them from EEG signals (Metsomaa et al., 2024). Data were re-referenced to the average, and ocular artifacts were suppressed. Removed channels were interpolated using spherical interpolation based on surrounding channels. Lastly, TMS–EEG trials from the same session were sorted according to experimental conditions: *sham* TMS pre-drug, *active* TMS pre-drug, *sham* TMS post-drug, *active* TMS post-drug.

2.6. SRT task

Scopolamine and biperiden could produce a sedative effect (Bakker et al., 2021). To assess this, we included an SRT task before and after drug administration. The SRT task measures how quickly a participant can respond when no other mental processing is required and is sensitive in detecting sedation (Baakman et al., 2017). During the task, a white square was displayed at the center of a screen at random intervals. Participants were instructed to press a button on a response box as quickly as possible whenever the square appeared. The inter-stimulus interval (ISI) was jittered between 500 and 1500 ms and uniformly distributed. We recorded reaction times from 40 trials per participant. Trials without button presses were excluded from further processing (1.3 % of trials across all participants). Additionally, we removed extreme values with SRTs shorter than 150 ms or longer than 700 ms (5.4 % of trials across all participants) (Karamacoska et al., 2018).

2.7. Data analysis

2.7.1. TEPs and sensory inputs-evoked EEG potentials (SEPs)

For each TMS target, we averaged TMS–EEG trials by experimental conditions per participant, resulting in *sham* TMS-evoked and *active* TMS-evoked EEG potentials separately for pre- and post-drug conditions. As previously reported (Gordon et al., 2023b; Song et al., 2023), the difference between *sham* TMS-evoked and *active* TMS-evoked EEG potentials reveals responses most likely due to direct cortical activation elicited by TMS. Therefore, in this study, we used the cleaned TEPs, obtained by subtracting the *sham* TMS-evoked from the *active* TMS-evoked EEG potentials, to represent genuine TEPs. Since the *sham* TMS consisted solely of multi-sensory inputs, the corresponding evoked EEG potential represented SEPs. Additionally, we projected the evoked sensor-level EEG potentials to source space using the L2-minimum-norm estimation (MNE) approach. More details are provided in Supplementary Materials: Section 1.2.

2.7.2. TIOs and sensory inputs-induced EEG oscillations (SIOs)

For each TMS target, we used the time-frequency representation (TFR) to obtain the power of stimulation-induced oscillations for each participant. We began by calculating trial-wise TFRs for each TMS–EEG trial and then averaged them by experimental conditions: *sham* TMS or *active* TMS, pre-drug or post-drug. These condition-averaged TFRs represented the total oscillatory power. Next, we computed TFRs for *sham* TMS-evoked and *active* TMS-evoked EEG potentials separately for pre-drug and post-drug conditions, which provided the *sham* TMS-evoked and *active* TMS-evoked oscillatory power, respectively. The *sham* TMS-induced and *active* TMS-induced oscillatory power were obtained by subtracting the evoked oscillatory power from the total power (Pellicciari et al., 2017). Specifically, for TFR calculation, we applied complex Morlet wavelet convolution to decompose the frequency band ranging from 4 to 40 Hz. The width of wavelets increased as a function of frequencies, with 2.6 cycles at 4 Hz and 7.1 cycles at 40 Hz linearly spaced by 0.12. We z-transformed the trial-wise TFRs using the mean and standard deviation of the full-length trial and performed baseline correction by subtracting the mean value of a pre-stimulus time window (−500 to −200 ms), following an established methodology (Belardinelli et al., 2021; Gordon et al., 2023b; Grandchamp and Delorme, 2011; Premoli et al., 2017). This ensured that the average pre-stimulation values did not differ from zero, allowing the z-values to be interpreted as modulation of the pre-stimulation oscillatory activity. To isolate the genuine TMS-induced oscillatory power, we used the cleaned TMS-induced oscillatory power, which was obtained by subtracting *sham* TMS-induced from *active* TMS-induced oscillatory power. As the *sham* TMS consisted solely of multisensory inputs, the corresponding oscillations represented SIOs.

2.7.3. Statistical analysis

Our study employed a within-subject 2-by-3 factorial design with two factors: *Time* (two levels: *PRE* and *POST*) and *Drug* (three levels: *PLA*, *BIP*, *SCO*) per TMS target.

Drug effects on TMS–EEG responses: Given the absence of strong prior hypotheses about the time/electrode/frequency window for analyzing the effects of anti-cholinergic drugs on TMS–EEG data, we chose the non-parametric cluster-based permutation test (Maris and Oostenveld, 2007). This method detects effects without being overly constrained by pre-specified theories and preserves the richness of high-dimensional EEG data (Fields and Kuperberg, 2020; Meyer et al., 2021). We incorporated cluster-based permutation tests into our multi-factorial design through a multi-step process. The pipeline was applied to TEPs, SEPs, TIOs, and SIOs separately. Fig. 2 illustrates an example in TEPs. We denoted the two levels of *Time* as T1 and T2 and the three levels of *Drug* as D1, D2, and D3. This created a six-cell data structure per TMS site (Fig. 2a): T1D1, T2D1, T1D2, T2D2, T1D3, and T2D3, and we assigned the condition-specific TEPs accordingly.

Our primary interest was the interaction effect of *Time* x *Drug*, i.e., whether the change in TEPs (ΔTEPs; Δ denotes *POST-PRE* difference) depended on the drug conditions. By iteratively subtracting TEPs in T2 from TEPs in T1, we reduced our design to one factor *Drug* with a three-

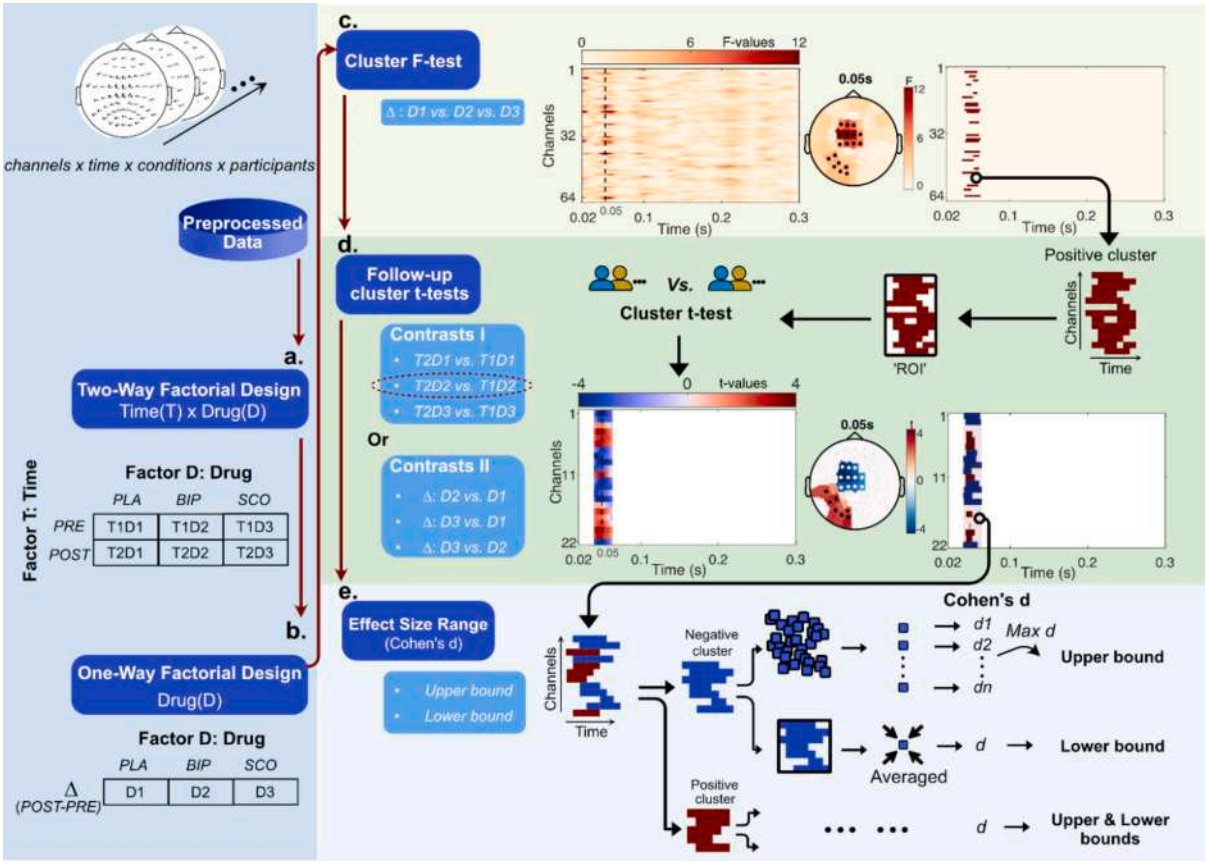

Fig. 2. Statistical analysis of TEPs. TEPs were derived by subtracting *sham* TMS-evoked potentials from *active* TMS-evoked EEG potentials, organized as channels x time x conditions x participants. (a) TEPs were sorted according to a Two-way factorial design: Factor A (Time) with levels T1 (PRE) and T2 (POST). Factor D (Drug) with levels D1 (PLA), D2 (BIP), and D3 (SCO). (b) Data was transformed into ΔTEP by subtracting PRE TEP from POST TEP, reducing the study into a One-way factor design: Factor D with levels D1 (PLA), D2 (BIP), and D3 (SCO). (c) A cluster-based permutation F-test was conducted on ΔTEPs among D1, D2, and D3. This assessed whether the change in TEPs (ΔTEPs) depended on the drug conditions, equivalent to testing a Time x Drug interaction effect. Sub-panels show F-values over time and channels (left), the F-value topography at 0.05 s with channels comprising the significant cluster marked in black (middle), and the spatiotemporal extent of the cluster (right). (d) Follow-up cluster-based permutation *t*-tests were performed within an ROI defined by the cluster identified in the F-test. Sub-panels display an example of the t-test result comparing T2D2 vs. T1D2: t-values showing over time and channels (left), the t-value topography at 0.05 s with channels comprising positive and negative clusters marked in black and white (middle), and the spatiotemporal extents of positive (in red) and negative (in blue) clusters (right). (e) Effect size range. For the upper bound, Cohen's d was calculated for each channel and time point within the cluster, and the largest value was eventually selected. For the lower bound, the cluster was circumscribed with a rectangular shape and Cohen's d was calculated for the averaged data within this shape. *Abbreviations: BIP, biperiden; PLA, placebo; PRE: pre-drug; POST: post-drug; SCO, scopolamine; ROI: region of interest; TEPs: TMS evoked EEG potentials.* (For interpretation of the references to colour in this figure legend, the reader is referred to the web version of this article.)

cell data structure (Fig. 2b): ΔTEPs for D1, D2, and D3. Conceptually, testing an interaction effect was equivalent to conducting an F-test on ΔTEPs among D1, D2, and D3, with the null hypothesis that ΔTEPs did not differ across conditions (Fields and Kuperberg, 2020). We employed the non-parametrical cluster-based permutation F-test, including all channels and a 20 to 300 ms post-stimulus time window (cluster threshold: $p < .025$ dependent F-test, critical $\alpha < 0.05$ one-tailed; randomization = 2000) (Fig. 2c). We chose $p < .025$ as cluster inclusion criteria, as TEPs, particularly in early latency, are short-lived and sharply peaked, and a more stringent criterion enhances sensitivity to focal effects (Fields and Kuperberg, 2020).

If a significant interaction effect was detected, we examined which drug condition primarily drove the interaction by testing planned contrasts (Fig. 2d: Contrast I). For instance, we compared T2D2 to T1D2 with the null hypothesis that they were not different. Importantly, these follow-up analyses were constrained to data within a region of interest (ROI), defined by a rectangular shape circumscribing the cluster identified by the F-test (Sassenhagen and Draschkow, 2019). For these follow-up analyses, we used non-parametric cluster-based permutation *t*-tests (cluster threshold: $p < .025$ dependent t-test, critical $\alpha < 0.05$ two-tailed; randomization = 2000) and corrected the critical alpha level for multiple comparisons using the Bonferroni approach (Tabachnick and Fidell, 2007). In the case of SEP, a significant difference between *POST* and *PRE* was identified in all drug conditions, including the placebo. This suggested that some time-varying factors, such as fatigue, might influence SEP over the course of the experiment (Boksem et al., 2005). To control this confounding effect, we directly compared ΔSEPs between drug conditions (Fig. 2d: Contrast II). For instance, we compared ΔSEPs under D2 to ΔSEPs under D1, with the null hypothesis that changes in SEPs were comparable between D1 and D2. To quantify the significant effects identified by cluster t-tests, we estimated the effect size using Cohen's d, which measures the standardized difference between means (Sawilowsky, 2009). Following Meyer et al. (Meyer et al., 2021), we reported an effect size range with an upper and lower bound (Fig. 2e). More details are provided in the Supplementary Materials: Section 1.3.

Similarly, we applied this pipeline to TIOs and SIOs, adjusting the parameters for the cluster-based F/t-tests to accommodate the three-dimensional data: channel x time x frequency. To examine if there was a *Time* x *Drug* interaction on oscillatory power, we conducted the cluster-based permutation F-test on Δpower (changes in oscillatory power; Δ denotes *POST-PRE* difference), including all channels, a time window of

50–650 ms and a frequency range of 4–40 Hz (cluster threshold: $p < .05$ dependent F-test, critical $\alpha < 0.05$ one-tailed; randomization = 2000). If a significant interaction effect was detected, we proceeded with follow-up analyses using cluster-based permutation t-tests (cluster threshold: $p < .05$ dependent t-test, critical $\alpha < 0.05$ two-tailed; randomization = 2000), and corrected the critical alpha level for multiple comparisons using the Bonferroni approach.

Drug effects on reaction time: We conducted a linear mixed-effects analysis on reaction time in R (version 4.3.2) using the lmer function from the lmerTest package:

$$1/\mathrm{SRT} \sim \mathrm{Time} + \mathrm{Drug} + \mathrm{Time} : \mathrm{Drug} + (1|\mathrm{participant})$$

Given that the data distribution of SRT was positively skewed, we applied a reciprocal transformation (−1/SRT) to the raw SRT data (Balota et al., 2013). The fixed effects in the model included the factors *Time* and *Drug*, as well as their interaction term *Time:Drug*. For random effects, we included intercepts for participants. If a significant *Time* x *Drug* interaction was found, we proceeded to test planned contrasts by comparing the estimated marginal means from *POST* versus *PRE* at each level of *Drug*. Multiple comparisons were controlled using the Bonferroni approach.

3. Results

3.1. Effects of drugs on reaction time

Visual inspection of residual plots from the model revealed mild deviations from normality. As outliers in the data may cause stress in the model, we further trimmed the data to exclude those with absolute standardized residuals exceeding 2.5 standard deviations (2.1 % of trials across all participants) (Baayen and Milin, 2010). The model built on the trimmed data had residuals that approximated normality more closely. The *Time* x *Drug* interaction effect on the transformed reaction time (−1/SRT) was significant ($p < .05$). Follow-up comparisons revealed that the interaction was driven by biperiden (*POST* vs. *PRE*, $p < .0001$, Cohen's d = 0.29) and scopolamine (*POST* vs. *PRE*, $p < .0001$, Cohen's d = 0.41) (Fig. 3).

3.2. Effects of drugs on TEPs

When stimulating the SMA, *POST-PRE* difference waveforms (ΔTEPs) and their respective topographies revealed prominent EEG features for the biperiden and scopolamine conditions (Fig. 4). The cluster-based permutation F-test revealed a significant difference in ΔTEPs among *PLA*, *BIP* and *SCO* (Table 1), suggesting a *Time* x *Drug* interaction. The difference was driven by the largest positive cluster ($p = .0351$, critical $\alpha = 0.05$), which approximately extended from 40 to 63 ms after the TMS pulse and covered 22 channels. Fig. 5a illustrates the cluster extent in time and channels, showing that the effect was more prominent at left parietal-central channels.

Given the presence of an interaction effect, we next investigated whether the interaction was driven more by scopolamine, biperiden, or both. Cluster-based permutation *t*-tests revealed that *POST* TEPs significantly differed from *PRE* only under the scopolamine condition (Table 2). The difference was driven by the largest negative cluster ($p = .0003$, corrected critical $\alpha = 0.0083$), approximately extending from 40 to 63 ms and spanning central channels (Fig. 5b). The estimated effect size range was large (Cohen's d = [0.82, 0.94]), yet relatively localized and short-lived, with its upper bound estimated at channel FC3 at 47 ms. As shown in Fig. 5b, the TEP at channel FC3 had a larger amplitude for *POST* scopolamine compared to *PRE* during the 40 to 63 ms window. Spatially, TEPs in the central areas were more negative after scopolamine administration, evident at both the sensor and source levels.

To assess if changes in TEPs correlated to changes in SRT under scopolamine at the group level, we used Spearman's correlation to calculate the relationship between the two variables. Changes in TEPs were averaged over the channels composing the cluster identified in the t-test, and changes in SRT were computed as means averaged over pre- and post-drug trials. We found no significant correlation between changes in SRT and changes in TEPs ($R_s = -0.28$, $p = .18$) (Supplementary Fig. 1).

The cluster-based permutation F-tests revealed no significant difference in ΔTEPs among *PLA*, *BIP* and *SCO* following either mPFC or AG stimulation (Table 1). This suggests an absence of *Time* x *Drug* interaction in TEPs when targeting these cortical areas (Supplementary Figs. 2 and 3). Consequently, no follow-up analyses were performed.

3.3. Effects of drugs on TIOs

We first aimed to characterize the TMS-induced oscillatory power for each TMS target by subtracting the effect of sensory inputs from the oscillatory response before any drug intervention (details of statistical analysis in Supplementary Materials: Section 1.4).

When stimulating the SMA, TMS-induced oscillatory power before drug administration was not significantly different across the three sessions (all identified clusters, $p > .05$). Therefore, we averaged the induced oscillator power before drug administration across three sessions to increase the signal-to-noise ratio (SNR). TMS over the SMA produced a power increase in the beta band at the left central channels, lasting up to around 200 ms (Fig. 6a). The cluster-based permutation *t*-test revealed that, when targeting the SMA, TMS-induced oscillatory power significantly differed from zero. The difference was driven by the positive cluster ($p = .0025$, Cohen's d = [0.61, 1.08], critical $\alpha = 0.025$), approximately extending from 11 to 40 Hz, 50 to 260 ms and spanning

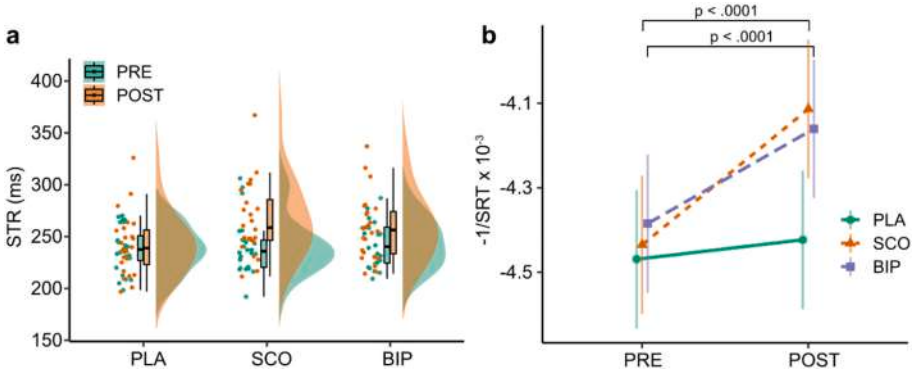

Fig. 3. Effects of drugs on reaction time. (a) Raincloud plot showing mean SRTs averaged across trials for each participant, with accompanying boxplots and probability densities for each condition. (b) Results from the linear mixed model on transformed trial-level data (−1/SRT), with estimated marginal means and 95 % confidence intervals for each condition. Significant *P*-values for the POST vs. PRE contrast are shown for SCO and BIP conditions. *Abbreviations: BIP, biperiden; PLA, placebo; SCO, scopolamine; PRE: pre-drug; POST: post-drug; SRT: simple reaction time.*

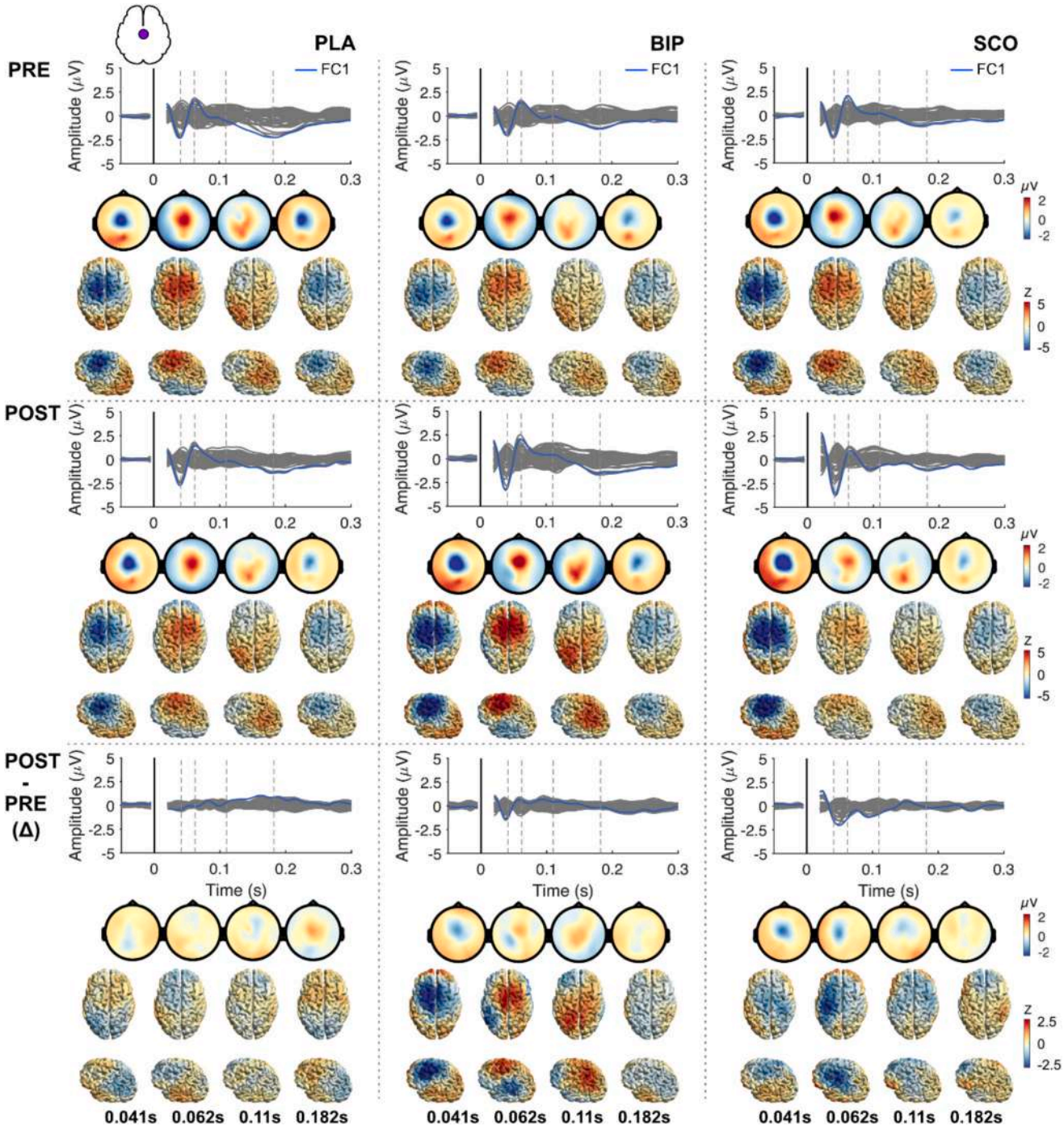

Fig. 4. TEPs in response to TMS of the SMA pre- and post-drug administration. TEPs were obtained by subtracting *sham* TMS-evoked from *active* TMS-evoked EEG potentials, averaged across participants. Each condition is shown by multi-channel TEP plots with topography time series displayed at both sensor and source levels. Rows: PRE, POST, and POST-PRE (Δ); Columns: PLA, BIP, and SCO. *Abbreviations: BIP, biperiden; PLA, placebo; PRE: pre-drug; POST: post-drug; SCO, scopolamine; SMA: supplementary motor area; TEPs: TMS evoked EEG potentials.*

54 channels (Fig. 6b). The estimated effect size was relatively large (Cohen's d = [0.61, 1.08]), with its upper bound estimated at 19 Hz, 60 ms, and channel FC3. However, when evaluating the drug effects on the TMS-induced power, the cluster-based permutation F-test revealed no significant difference in Δpower among *PLA*, *BIP,* and *SCO*, indicating the absence of *Time* x *Drug* interaction. Consequently, no follow-up analyses were performed.

When targeting the mPFC and AG, the corresponding TMS-induced oscillatory power before drug administration was not significantly different from zero (all identified clusters, $p > .025$). This indicates that TMS did not elicit robust oscillatory power in these cortical regions (Supplementary Fig. 4). Consequently, we did not proceed with further analyses of drug effects on TIOs from mPFC and AG stimulations.

3.4. Effects of drugs on SEPs

SEPs before drug administration were not significantly different among the three sessions (all identified clusters, $p > .05$). SEP waveforms and topographies were similar across sessions, with the typical N100–P200 complex evident at the frontal-central channels (Fig. 7).

Table 1
Cluster-based permutation F-test results on ΔTEPs among PLA, BIP, and SCO, separately for TMS of the SMA, AG, and mPFC.

	Cluster		Approximate extent	
SMA	Polarity	P-value	Time [ms]	Space [N channels]
Δ: PLA vs. BIP vs. SCO	+	**0.0351**	40–63	22
AG				
Δ: PLA vs. BIP vs. SCO	+	0.3986		
mPFC				
Δ: PLA vs. BIP vs. SCO	+	0.0898		

Only clusters with the smallest p-value are listed. The cluster with a *p*-value less than the critical **α (= 0.05)** is highlighted in bold, along with its approximate spatiotemporal extent. ΔTEP represents the changes in TEPs between post- and pre-drug administrations. TEPs were obtained by subtracting *sham* TMS-evoked from *active* TMS-evoked EEG potentials. *Abbreviations: AG: angular gyrus; BIP, biperiden; mPFC: medial prefrontal cortex; PLA, placebo; SCO, scopolamine; SMA, supplementary motor area; TEPs: TMS evoked EEG potentials.*

POST-PRE difference waveforms (ΔSEPs) and their corresponding topographies resembled N100–P200 but with reversed polarities, indicating that N100 was less negative and P200 was less positive after drug administration. This pattern was observed across all drug conditions, including the placebo. The cluster-based permutation F-test revealed significant differences in ΔSEPs among *PLA*, *BIP* and *SCO* (Table 3). These differences were driven by two positive clusters identified in the observed data (Table 3). The largest cluster ($p = .0001$, critical $\alpha = 0.05$) indicated a late-onset interaction effect from about 208 to 300 ms post-stimulus. The second largest cluster ($p = .0006$, critical $\alpha = 0.05$) indicated a relatively early interaction effect from around 34 to 120 ms (Fig. 8a). In follow-up analyses, we compared ΔSEPs between drugs (Table 4) separately within the two time windows.

During the early time window, ΔSEPs caused by scopolamine differed significantly from placebo, while no significant differences were found between biperiden and placebo or between scopolamine and biperiden (Table 4). The differences were driven by a negative and a positive cluster (Neg: $p = .0001$, Cohen's d = [1.24, 1.35]; Pos: $p = .0001$, Cohen's d = [1.06, 1.08], corrected critical $\alpha = 0.0042$), occurring from about 38 to 118 ms (Fig. 8b). During the late time window, ΔSEPs caused by biperiden differed significantly from both placebo and scopolamine (Table 4). The biperiden vs. placebo contrast revealed significant differences driven by a negative and a positive cluster (Neg: $p = .0001$, Cohen's d = [0.96, 1.08]; Pos: $p = .0015$, Cohen's d = [0.91, 1.06], corrected critical $\alpha = 0.0042$), occurring from about 208 to 263 ms (Fig. 8c). Similarly, the biperiden vs. scopolamine contrast revealed significant differences driven by a negative and a positive cluster (Neg: $p = .0012$, Cohen's d = [1.09, 1.17]; Pos: $p = .0005$, Cohen's d = [0.69, 1.13], corrected critical $\alpha = 0.0042$), occurring from around 208 to 300 ms (Fig. 8d).

3.5. Effects of drugs on SIOs

The sensory inputs-induced oscillatory power before drug administration was not significantly different across the three sessions (all identified clusters, $p > .05$). Fig. 9a illustrates the induced power before drug administration averaged across sessions, revealing a triphasic pattern: a brief power increase (enhancement) in broadband oscillations, followed by a decrease (suppression) and a subsequent rebound in

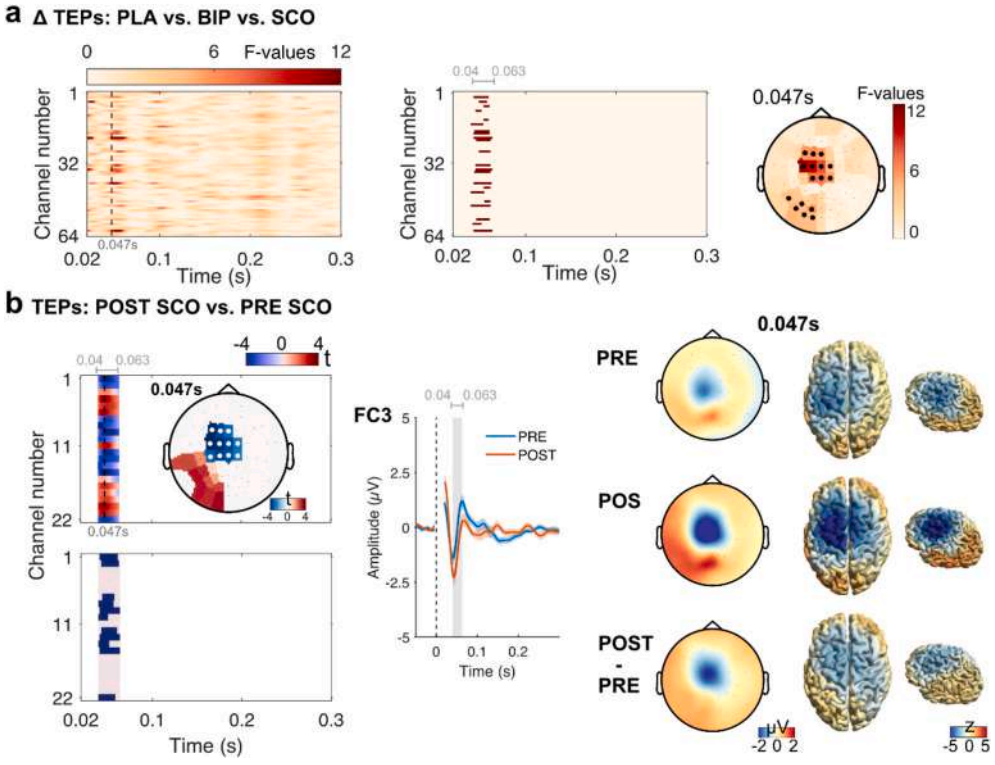

Fig. 5. Effects of drugs on TEPs in response to TMS of the SMA. (a) Cluster F-test results on ΔTEPs among PLA, BIP, and SCO. Sub-panels show F-values over time and channels (left), the spatiotemporal extent of the significant cluster (middle), and the F-value topography at 0.047 s with channels comprising the significant cluster marked in black (right). (b) Cluster *t*-test results comparing TEPs for POST SCO vs. PRE SCO. The left sub-panel displays t-values over time and channels and the t-value topography at 0.047 s, with channels comprising the significant cluster marked in white (top) and the spatiotemporal extent of the significant cluster (bottom). The middle sub-panel shows the TEP from channel FC3 with ±standard error of the means. The right sub-panel shows the topography of TEPs at 0.047 s at both sensor and source levels. The selected timepoint and channel correspond to the sample yielding the upper bound of effect size (Table 2). *Abbreviations: BIP, biperiden; PLA, placebo; PRE: pre-drug; POST: post-drug; SCO, scopolamine; SMA: supplementary motor area; TEPs: TMS evoked EEG potentials.*

Table 2
Cluster-based permutation t-test results comparing SMA TEPs for POST vs. PRE, separately for each drug condition.

Within 40–63 ms						
	Clusters		Approximate extent		Effect size	
Contrasts I	Polarity	P-value	Time [ms]	Space [N channels]	Range	Channel-time pair
PLA: POST vs. PRE	+	0.0487				
BIP: POST vs. PRE	+	0.0466				
	−	0.0098				
SCO: POST vs. PRE	+	0.0116				
	−	**0.0003**	40–63	11	0.82–0.94	FC3; 47 ms

Only clusters with the smallest p-value are listed. The cluster with a p-value less than the critical **α (= 0.0083**, Bonferroni corrected**)** is highlighted in bold, along with its approximate spatiotemporal extent and effect size range. The channel-time pair corresponds to the sample yielding the upper bound of the effect size. TEPs were obtained by subtracting evoked EEG potentials to *sham* from those to *active* TMS. *Abbreviations: BIP, biperiden; PLA, placebo; PRE: pre-drug; POST: post-drug; SCO, scopolamine; SMA, supplementary motor area; TEPs: TMS evoked EEG potentials.*

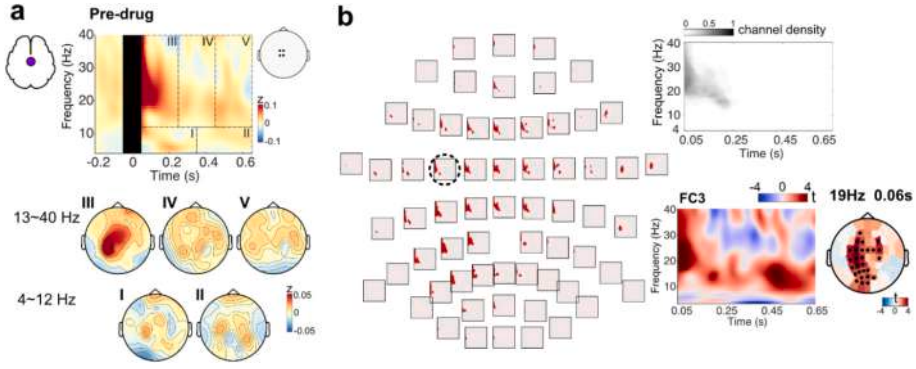

Fig. 6. TMS-induced oscillatory power in response to SMA stimulation pre-drug administration. The power was derived by subtracting *sham* TMS-induced from *active* TMS-induced EEG oscillatory power. (a) TFRs pre-drug administration were averaged across participants, channels underneath the coil (FCz, FC1, Cz, C1), and the three sessions. The black box masks the time window (−0.05 to 0.05 s) potentially contaminated by TMS-related artifacts. The bottom rows show topographies of the induced power, averaged across five time-frequency regions of interest chosen based on visual inspection (I: 0.05–0.35 s; II: 0.36–0.65 s; III: 0.05–0.25 s; IV: 0.26–0.45 s; V: 0.46–0.65 s). (b) Cluster t-test results comparing TMS-induced oscillatory power pre-drug administration against zero. The left sub-panel shows the spectral-temporal extent of the significant cluster according to electrode layout. The right sub-panel shows the ratio of channels comprising the significant cluster to the total number of channels (top), t-values over time and frequencies at channel FC3, and the t-value topography at 19 Hz, 0.06 s (bottom). The selected time point, channel, and frequency correspond to the sample yielding the upper bound of effect size. *Abbreviations: SMA, supplementary motor area; TFRs: time-frequency representations.*

power (enhancement), more prominently in the higher frequency range.

Following drug administrations, the induced power showed distinct alterations (Fig. 9b). The cluster-based permutation F-test revealed a significant difference in Δpower among *PLA*, *BIP,* and *SCO* (Table 5). This difference was driven by a positive cluster ($p = .0005$, critical $\alpha = 0.05$), indicating a *Time* x *Drug* interaction effect extending globally from 4 to 40 Hz, 50 to 650 ms and encompassing all channels. To determine whether the interaction was driven more by scopolamine, biperiden, or both, we conducted cluster-based permutation *t*-tests. We found that, unlike placebo, both scopolamine and biperiden significantly increased the induced oscillatory power (Table 6). Specifically, the *POST* vs. *PRE* contrast under biperiden revealed a significant difference driven by a positive cluster ($p = .0010$, Cohen's d = [0.5, 1.23], corrected critical $\alpha = 0.0083$), approximately extending from 4 to 33 Hz, 50 to 650 ms, and covering all channels (Fig. 9c). Similarly, the *POST* vs. *PRE* contrast under scopolamine revealed a significant difference driven by a positive cluster ($p = .0005$, Cohen's d = [0.89, 1.53], corrected critical $\alpha = 0.0083$), extending globally from 4 to 33 Hz, 50 to 650 ms, and converging all channels (Fig. 9d). While both scopolamine and biperiden had widespread effects on induced oscillatory power in terms of spatial and spectral distribution, their effects displayed distinct features. Biperiden primarily reversed the power suppression induced by sensory stimulation, whereas scopolamine appeared to augment power enhancements in both the early low-frequency and later higher-frequency ranges.

4. Discussion

The involvement of neuromodulator-mediated neurotransmission in TMS–EEG responses remains largely unexplored. In this study, we investigated how the inhibition of mAChR-mediated cholinergic neurotransmission through the intake of mAChR antagonists scopolamine and biperiden affects TEPs and TIOs. There are three main findings in this study: 1) TEPs are affected by the inhibition of cholinergic neurotransmission, with significant effects observed specifically when scopolamine is used and TMS targets the SMA. 2) While cholinergic inhibition also modulates SEPs, its effects on TEPs are independent of those on SEPs. 3) The power of SIOs, but not TIOs, is increased by the inhibition of cholinergic neurotransmission. Both scopolamine and biperiden significantly enhance broadband synchronization, each with distinct profiles.

4.1. mAChR-mediated cholinergic transmission in TMS–EEG responses when targeting the SMA

In our study, TMS over the SMA produces an N45-like TEP component near the stimulation site. Its amplitude increased significantly following scopolamine administration, with biperiden showing a similar but less robust effect (Fig. 4). The N45 component is thought to reflect the balance of excitatory and inhibitory neurotransmission, as supported by previous pharmacological TMS–EEG studies targeting the M1. These studies have shown that the amplitude of N45 increases by diazepam, a

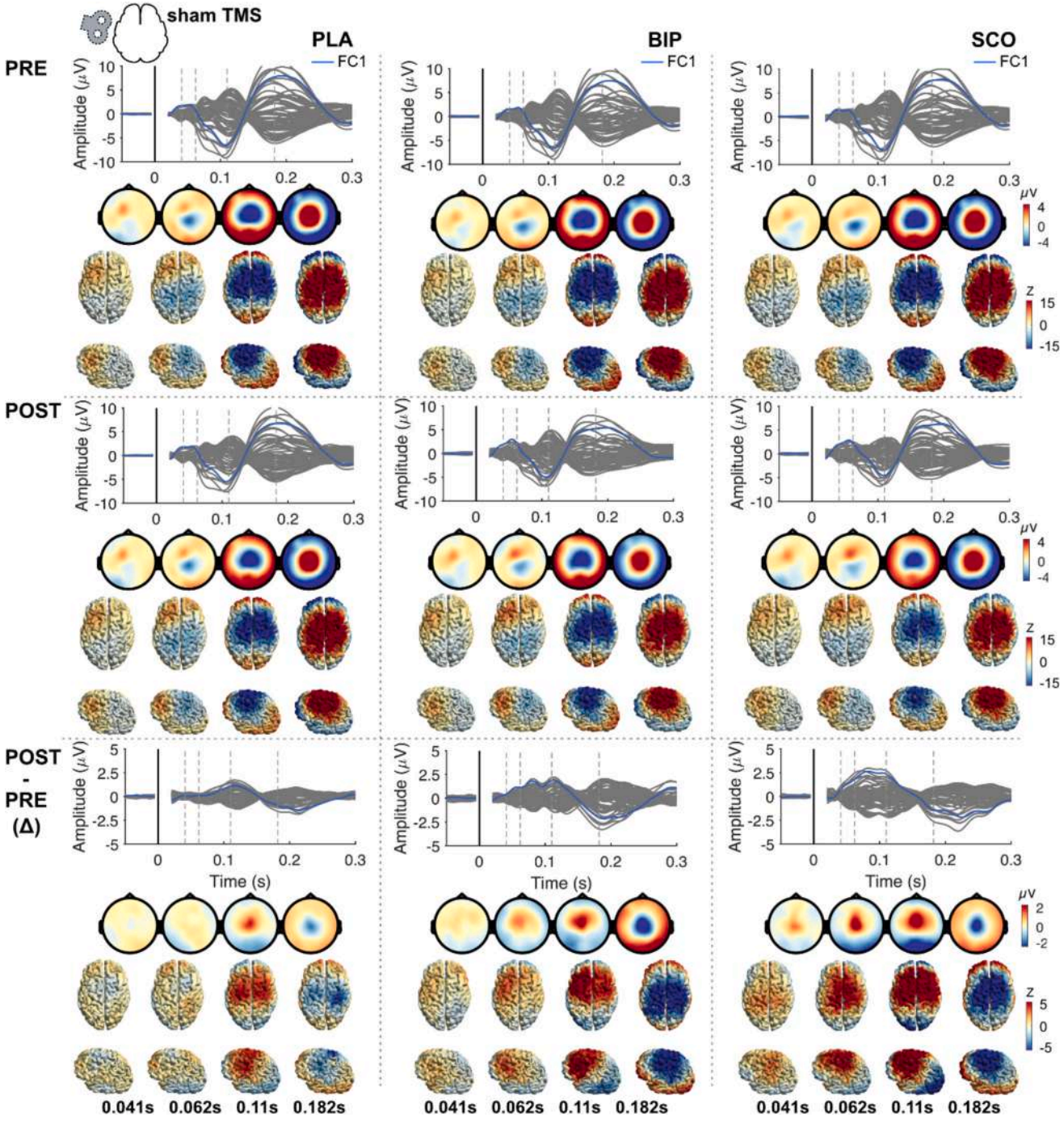

Fig. 7. SEPs in response to *sham* TMS stimulation. SEPs were averaged across participants. Each condition is shown by multi-channel SEP plots with topography time series displayed at both sensor and source levels. Rows: PRE, POST, and POST-PRE (Δ); Columns: PLA, BIP, and SCO. *Abbreviations: BIP, biperiden; PLA, placebo; PRE: pre-drug; POST: post-drug; SCO, scopolamine; SEPs: sensory inputs evoked EEG potentials.*

Table 3
Cluster-based permutation F-test result on ΔSEPs among PLA, BIP, and SCO.

	Clusters		Approximate extent	
	Polarity	P-value	Time [ms]	Space [N channels]
Δ: PLA vs. BIP vs. SCO	+	**0.0001**	208–300	50
	+	**0.0006**	34–120	37

Clusters with *p*-values less than the critical **α (= 0.05)** are listed, along with their approximate spatiotemporal extents. ΔSEP represents the changes in SEPs between post- and pre-drug administrations. *Abbreviations: BIP, biperiden; PLA, placebo; SCO, scopolamine; SEPs: sensory inputs evoked EEG potentials.*

positive allosteric modulator at GABAARs, and dextromethorphan, a competitive antagonist at the NMDAR (Belardinelli et al., 2021; Premoli et al., 2014), while it decreases by compound S44819, an experimental compound acting as specific antagonist at the alpha5-GABAAR (Darmani et al., 2016). Therefore, the increased N45 amplitude in our study likely indicates a shift of the excitation / inhibition balance, possibly toward more inhibition, following anti-cholinergic intervention.

While other cortical regions may also contribute, N45 is likely caused by activation of a cortical-subcortical motor circuit (Ziemann et al., 2015), such as the corticobasal ganglia-thalamo-cortical loop. Cortical

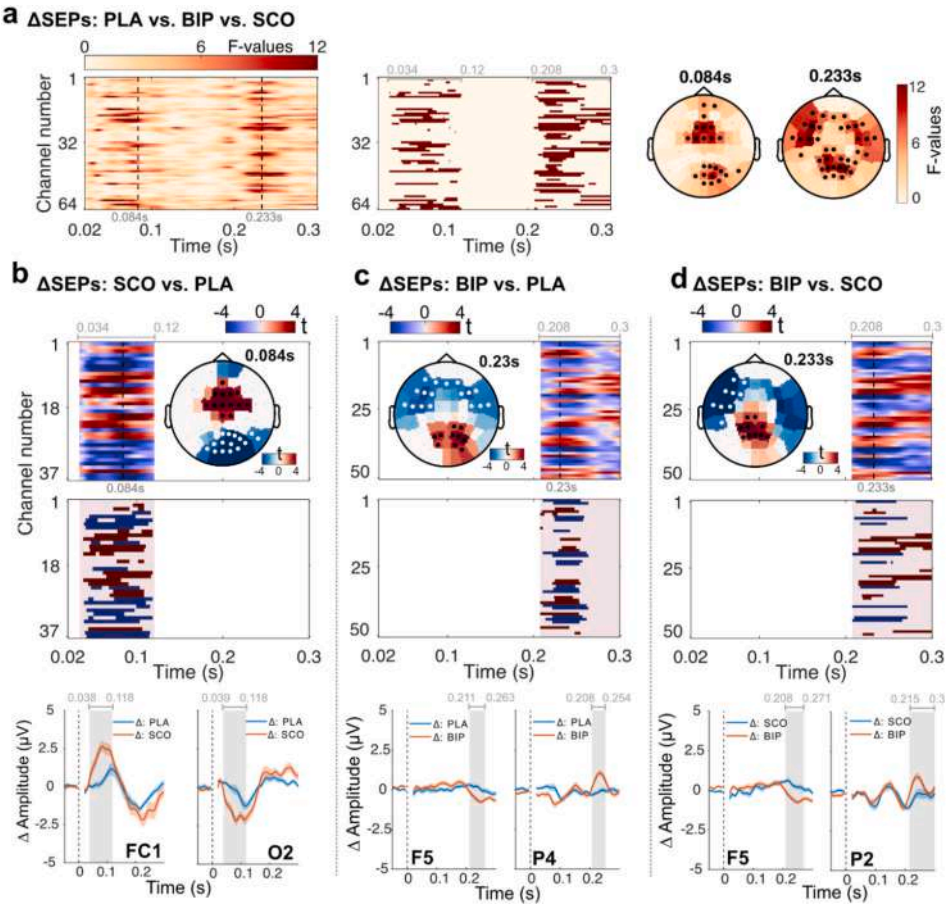

Fig. 8. Effects of drugs on SEPs in response to *sham* TMS stimulation. (a) Cluster F-test results on ΔSEPs among PLA, BIP, and SCO. Sub-panels show F-values over time and channels (left), the spatiotemporal extent of the two significant clusters (middle), and the F-value topography at 0.084 s and 0.233 s with channels comprising the significant clusters marked in black (right). Cluster t-test results comparing ΔSEPs for (b) SCO vs. PLA, (c) BIP vs. PLA, and (d) BIP vs. SCO. Within each panel, the top sub-panel shows t-values over time and channels and the t-value topography at a selected time point, with channels comprising the significant positive and negative clusters marked in black and white. The middle sub-panel shows the spatiotemporal extent of the significant positive (in red) and negative (in blue) clusters. The bottom sub-panel shows grand average ΔSEPs from selected channels with ±standard error of the means. The selected timepoint and channel correspond to the sample yielding the upper bound of effect size (Table 4); *Abbreviations: BIP, biperiden; PLA, placebo; SCO, scopolamine; SEPs: sensory inputs evoked EEG potentials.* (For interpretation of the references to colour in this figure legend, the reader is referred to the web version of this article.)

motor areas are interconnected with basal ganglia (BG) structures, such as the striatum and the subthalamic nucleus (STN). In these regions, synapses are formed with glutamatergic inputs from the cortex and dopaminergic inputs from the midbrain, which then relay information back to the cortex via the thalamus (Nakano et al., 2000; Utter and Basso, 2008). The SMA is a primary target of this BG motor circuit through the thalamus (Utter and Basso, 2008). During deep brain stimulator implantation surgery in PD patients, single-pulse TMS over the M1 altered the firing rate of STN neurons (Strafella et al., 2004), and TMS over the SMA and M1 produced evoked local field potentials recorded at the level of the STN (Doyle Gaynor et al., 2008). These studies confirm that excitation from stimulated motor areas can descend through cortical-subcortical tracts. Furthermore, ascending information from subcortical to motor cortical areas is supported by deep brain stimulation studies, where evoked EEG potentials were recorded from scalp electrodes in the motor cortical area following basal ganglia stimulation (STN or internal globus pallidus) (Kuriakose et al., 2010; Ni et al., 2018; Walker et al., 2012), with positive or negative peaks at varied latencies (<10 ms or 20–25 ms).

This circuitry is a complex network where glutamatergic (excitatory) and GABAergic (inhibitory) neurotransmission transsynaptically convey information, finely regulated by multiple neuromodulators (Augustine and Singer, 2018). Among these, AChR-mediated cholinergic transmission plays an important modulating role. Striatal cholinergic interneurons are tonically active, releasing ACh spontaneously in the absence of synaptic input (Abudukeyoumu et al., 2019). mAChRs are highly expressed by axon terminals of major afferents to the striatum (glutamatergic and dopaminergic terminals) and by striatal neurons, including (GABAergic) medium spiny projection neurons and other interneurons (Ztaou and Amalric, 2019). The diverse distribution of mAChRs and the autonomous firing feature of cholinergic interneurons underpin cholinergic regulation of striatal output, affecting medium spiny projection neurons directly and indirectly by modulating dopamine, glutamate, and GABA release (Abudukeyoumu et al., 2019; Ztaou and Amalric, 2019). One pharmacological TMS–EEG study investigated whether the acute intake of the dopamine precursor levodopa affected TEPs when targeting the SMA (Casarotto et al., 2019). They quantified TEPs using local mean field power in channels near the SMA within a time window of about 15 to 60 ms. Their findings showed that levodopa increased the size of TEPs, similar to the effect of the mAChR antagonist scopolamine observed in our study. These observations align with the known interplay between cholinergic and dopaminergic systems in basal ganglia function, where cholinergic tone increases as striatal dopamine levels decline, and vice versa (Aosaki et al., 2010). While delineating the exact neurotransmission processes affected by cholinergic inhibition is beyond the scope of our study, our findings suggest that striatal cholinergic signaling likely regulates the BG-thalamo-cortical pathway, thereby tuning excitatory and inhibitory transmission and, ultimately,

Table 4
Cluster-based permutation *t*-test results comparing ΔSEPs between drugs within two time windows.

Within 34–120 ms						
	Clusters		Approximate extent		Effect size	
Contrasts II	Polarity	P-value	Time [ms]	Space [N channels]	Range	Channel-time pair
Δ: SCO vs. PLA	+	**0.0001**	38–118	16	1.06–1.08	FC1; 84 ms
	−	**0.0001**	39–118	17	1.24–1.35	O2; 88 ms
Δ: BIP vs. PLA	+	0.0310				
	−	0.0224				
Δ: SCO vs. BIP	+	0.1937				
	−	0.0217				

Within 208–300 ms						
	Clusters		Approximate extent		Effect size	
Contrasts II	Polarity	P-value	Time [ms]	Space [N channels]	Range	Channel-time pair
Δ: SCO vs. PLA	+	0.1418				
	−	0.0504				
Δ: BIP vs. PLA	+	**0.0015**	208–254	15	0.91–1.06	P4; 230 ms
	−	**0.0001**	211–263	17	0.96–1.08	F5; 242 ms
Δ: BIP vs. SCO	+	**0.0005**	215–300	18	0.69–1.13	P2; 233 ms
	−	**0.0012**	208–271	9	1.09–1.17	F5; 248 ms

Only clusters with the smallest p-value are listed. The clusters with p-values less than the critical **α (= 0.0042**, Bonferroni corrected**)** are highlighted in bold, along with their approximate spatiotemporal extent and effect size range. The channel-time pair corresponds to the sample yielding the upper bound of the effect size. ΔSEP represents the changes in SEPs between post- and pre-drug administrations. *Abbreviations: BIP, biperiden; PLA, placebo; SCO, scopolamine; SEPs: sensory inputs evoked EEG potentials.*

influencing the excitability of the SMA.

In addition to these observations on TEPs, we found that TMS over the SMA induces a significant power increase in the 11–40 Hz range, representing beta/gamma band synchronization. This spectral dynamic of TIOs is consistent with a previous study that observed a similar oscillatory profile when TMS was applied to the cortical Brodmann area 6 (the middle or caudal portion of the superior frontal gyrus) (Rosanova et al., 2009). It has been suggested that such TMS-related oscillatory activity represents the natural frequency of the stimulated cortico-thalamic circuit. However, unlike TEPs, we did not observe anti-cholinergic modulation of TMS-induced oscillatory power, suggesting that mAChR-mediated cholinergic neurotransmission is less involved in TIOs. This discrepancy corroborates the notion that different neuro-physiological mechanisms underlie non-phase-locked TIOs and phase-locked TEPs.

4.2. mAChR-mediated cholinergic transmission in TMS–EEG responses when targeting the mPFC and AG

We found no significant effects of anti-cholinergic drugs on TEPs when stimulating the mPFC and AG. This suggests that mAChR-mediated cholinergic transmission likely does not contribute to TEPs when applying TMS to these regions in a task-free state (i.e., at rest). The primary source of ACh in the neocortex are BF cholinergic neurons. Although mAChRs are widespread across the cortex, ACh release from the BF to the cortex is region-specific and context-dependent. This specificity is possibly due to BF cholinergic neurons being organized in groups and active according to both topographical and functional principles, resulting in the spatiotemporal precision of BF cholinergic signaling (Muñoz and Rudy, 2014; Záborszky et al., 2018). Animal studies using microdialysis have shown that ACh release in the mPFC and parietal regions is specifically associated with cue detection and goal-oriented processes but not with basic behavioral operations that are not explicitly attention-demanding (Arnold et al., 2002; Himmelheber et al., 1997; Parikh et al., 2007). Similarly, in a human fMRI study, it was demonstrated that scopolamine intake can reduce brain activation in the left superior and middle frontal regions during an attentional reorienting task (Thienel et al., 2009). It is also possible that nAChR-mediated, rather than mAChR-mediated, cholinergic transmission might play a significant role. Hyperactivations in medial frontoparietal regions secondary to nicotine (a nAChR agonist) intake were observed in the resting state and in a task with low attention requirements (Lawrence et al., 2002; Stein et al., 1998). Future research may explore to what extent mAChR-mediated or nAChR-mediated cholinergic neurotransmission is involved in TMS–EEG responses in the context of attention tasks. Lastly, as we previously reported (Song et al., 2023), TMS over the mPFC resulted in a higher degree of variability in TEPs between individuals and across repeated sessions in the same individuals than the SMA and AG, which may have hindered the discovery of drug effects. However, this explanation does not entirely account for the absence of drug effects during AG stimulation.

4.3. mAChR-mediated cholinergic transmission in sensory-related EEG responses

Our study shows that the inhibition of cholinergic transmission affects cortical EEG responses to auditory and somatosensory stimuli associated with TMS. Moreover, these effects vary depending on the specific mAChRs being blocked, as evidenced by the distinct changes in SEPs and SIOs by scopolamine and biperiden.

The impact of cholinergic signaling on sensory processing is often examined in the context of cognitive functions such as attention and memory, where sensory stimuli can be either relevant or irrelevant to a task (Bentley et al., 2011). Previous studies on the effects of scopolamine or biperiden on event-related potentials in response to sensory stimuli have shown mixed results across varied task paradigms (e.g., passive exposure or attention-demanding) and sensory cues (e.g., visual, auditory, somatosensory, or multimodal) (reviewed in (Kunnath et al., 2023)). Some studies report decreases in the amplitudes of components like P50, N1, P1, P2, and P3a, while others report no changes or even opposite effects. In our study, we used cluster-based permutation F/*t*-tests to analyze changes in SEPs (ΔSEPs), rather than examining SEPs at pre-selected channels and time points, which makes direct comparisons with previous literature challenging. However, we observed that the amplitudes of the N100 and P200 components at frontal-central channels were more reduced under the influence of scopolamine and

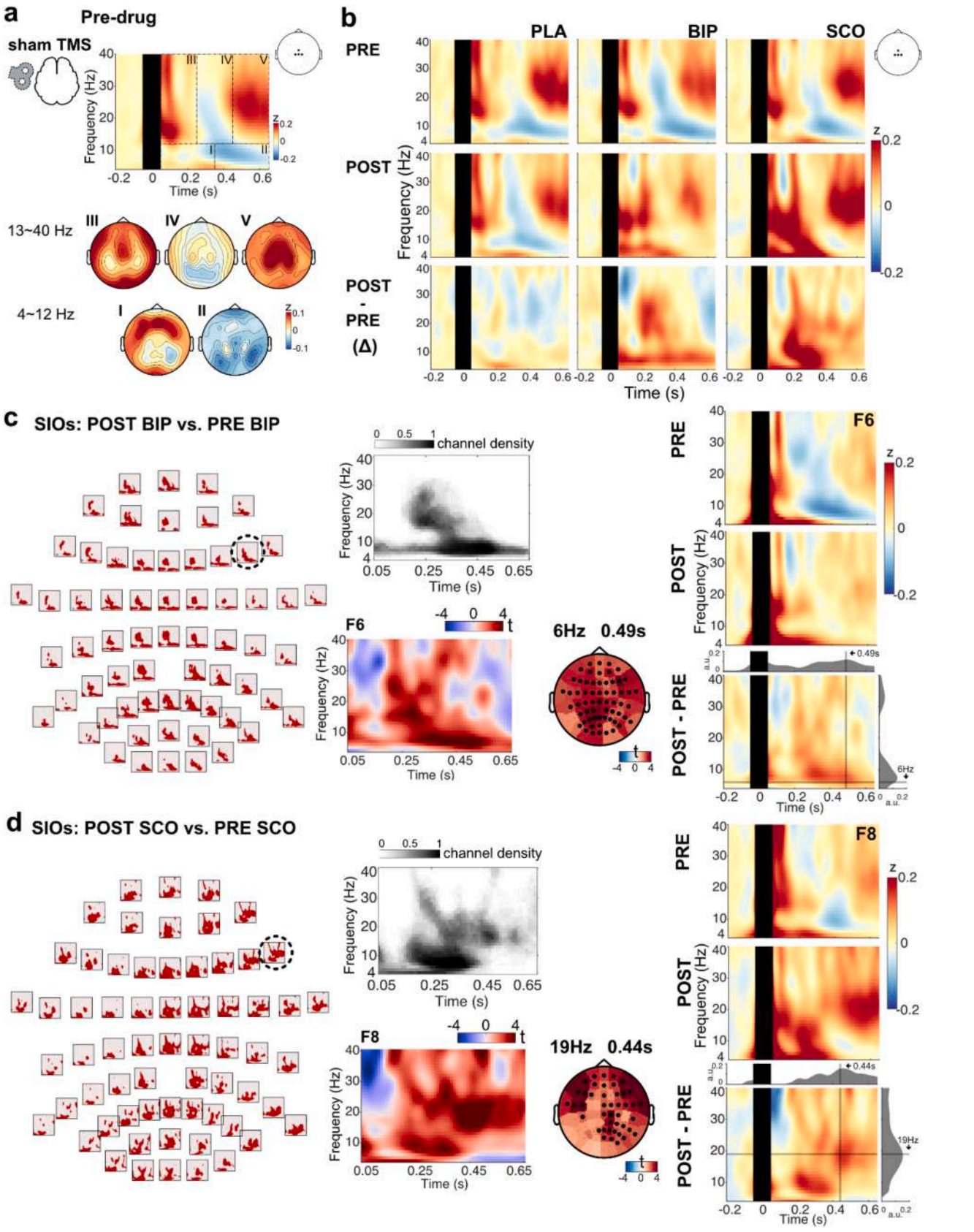

(caption on next page)

Fig. 9. Sensory inputs-induced oscillatory power in response to *sham* TMS stimulation (a) TFRs pre-drug administration were averaged across participants, channels (FCz, Cz, C1, C2), and the three sessions. The black box masks the time window (−0.05 to 0.05 s) potentially contaminated by stimulation-related artifacts. The bottom rows show topographies of the induced power, averaged across five time-frequency regions of interest chosen based on visual inspection (I: 0.05–0.35 s; II: 0.36–0.65 s; III: 0.05–0.25 s; IV: 0.26–0.45 s; V: 0.46–0.65 s). (b) Condition-specific TFRs, averaged across participants and channels (FCz, Cz, C1, C2). Rows: PRE, POST, and POST-PRE (Δ); Columns: PLA, BIP, and SCO. Cluster t-test results comparing the induced oscillatory power for (c) BIP: POST vs. PRE and (d) SCO: POST vs. PRE. Within each panel, the left sub-panel shows the spectral-temporal extent of the significant positive cluster according to electrode layout. The middle sub-panel shows the ratio of channels comprising the significant cluster to the total number of channels (top), t-values over time and frequencies at a selected channel, and the t-value topography at a selected frequency-time (bottom). The right sub-panel shows TFRs from a selected channel at PRE, POST, and POST-PRE. Marginal plots in the POST-PRE plot depict the power of a selected frequency change over time (top), and the power at a selected time point change over frequency (right). The selected time points, channels, and frequencies correspond to the sample yielding the upper bound of effect size (Table 6). *Abbreviations: BIP, biperiden; PLA, placebo; PRE: pre-drug; POST: post-drug; SCO, scopolamine; SIOs: sensory inputs-induced EEG oscillations; TFRs: time-frequency representations.*

Table 5
Cluster-based permutation F-test result on Δsensory inputs-induced oscillatory power among PLA, BIP, and SCO.

	Clusters		Approximate extent		
	Polarity	P-value	Freq [Hz]	Space [N channels]	Time [ms]
Δ: PLA vs. BIP vs. SCO	+	**0.0005**	4–40	64	50–650

The cluster with a p-value less than the critical **α (= 0.05)** is listed, along with its approximate spectral-spatial-temporal extent. Δ represents the changes in oscillatory power between post- and pre-drug administrations. *Abbreviations: BIP, biperiden; PLA, placebo; SCO, scopolamine.*

biperiden compared to the placebo (Fig. 7), aligning with studies reporting decreased N1 and P2 amplitudes (Caldenhove et al., 2017; Curran et al., 1998).

Regarding SIOs, we observed a typical pattern of oscillatory power elicited by sensory inputs: a brief broadband synchronization, followed by alpha/beta band desynchronization, and a subsequent rebound (synchronization) in the beta band. This spectral profile is commonly observed in magnetoencephalography (M/EEG) studies, with variations depending on stimulus modality and time-frequency analysis methods (Andersen and Lundqvist, 2019; Bauer et al., 2006; Novembre et al., 2019). We found that anticholinergic drugs significantly alter spectral dynamics (Fig. 9): biperiden primarily reverses alpha/beta band desynchronization, while scopolamine appears to enhance synchronization in both the alpha band early after stimulation and the beta band at a later period. Consistent with our findings, optogenetic studies in animals demonstrated that cholinergic signaling activation from the BF to sensory cortices causes desynchronization, while inhibition of cholinergic signaling enhances synchronization (Kim et al., 2016; Pinto et al., 2013).

Overall, our results support the notion that ACh in the sensory cortex influences sensory processing by altering neuronal responses to specific stimuli, shifting cortical dynamics from synchronous to asynchronous (Colangelo et al., 2019; Záborszky et al., 2018). Moreover, we found that sensory-related responses are differentially affected by scopolamine and biperiden. Biperiden differs from scopolamine in its binding specificity to M1 mAChR, compared to scopolamine's non-selective action on mAChRs. While M1–M4 mAChRs are widely expressed in the cortex, their distributions are layer- and cell-type specific. Such specificity is believed to be one reason that neural populations receiving the same sensory input could respond differentially (Colangelo et al., 2019; Thiele, 2013). Thus, distinct changes in sensory responses could be observed depending on which mAChR was blocked.

4.4. Control for TMS-associated sensory inputs

Anti-cholinergic drugs affect sensory-related EEG responses to *sham* TMS, a control condition that includes TMS-associated somatosensory and auditory inputs. These changes could be misinterpreted as anti-cholinergic modulation of genuine TEPs if sensory EEG components are not isolated before evaluating drug effects. To address this, we evaluated drug effects on cleaned TMS–EEG responses by subtracting the *sham* TMS-related EEG responses from those in the *active* TMS condition. The necessity of controlling sensory input in pharmacological TMS–EEG studies was highlighted in our recent study (Gordon et al., 2023b), where the N100 component identified in both *sham* and *active* TMS-evoked EEG potentials was affected by diazepam intake. However, in the cleaned TEPs, where the *sham* TMS-evoked EEG potentials were removed, the N100 component was largely attenuated and insensitive to diazepam. This suggests that the N100 component originates from sensory activation, and its modulation by diazepam should be interpreted as drug effects on sensory processing.

Furthermore, the profile of sensory input-induced oscillatory power, as shown in TFR plots (Fig. 9), can also be observed in the *sham* TMS condition (Gordon et al., 2023b), as well as in several TMS–EEG studies where TMS was applied to different cortical regions (Biondi et al., 2022; Casula et al., 2016; Premoli et al., 2017). This similarity suggests that some of the oscillatory power observed in these studies may stem from TMS-associated sensory inputs rather than direct cortical responses.

Controlling for TMS-associated sensory inputs is necessary for studies using TMS–EEG to measure cortical responsiveness before and after an intervention. Despite constant stimulation parameters before and after the intervention on the same participant, sensory processing can be modulated by the intervention itself, complicating the interpretation of EEG responses. Without proper sensory control, it becomes challenging to determine to what extent observed changes in EEG responses are due to the intervention's effect on direct cortical activation

Table 6
Cluster-based permutation *t*-test results comparing the sensory inputs-induced oscillatory power for POST vs. PRE for each drug condition.

	Clusters		Approximate extent			Effect size	
Contrasts I	Polarity	P-value	Freq [Hz]	Space [N channels]	Time [ms]	Range	Channel-freq-time triplet
PLA: POST vs. PRE	+	0.7206					
	−	0.0785					
BIP: POST vs. PRE	+	**0.0010**	4–33	64	50–650	0.50–1.23	F6; 6 Hz; 490 ms
	−	0.0725					
SCO: POST vs. PRE	+	**0.0005**	4–40	64	50–650	0.89–1.53	F8; 19 Hz; 440 ms
	−	0.1754					

Only clusters with the smallest p-value are listed. The clusters with *p*-values less than the critical **α (= 0.0083**, Bonferroni corrected**)** are highlighted in bold, along with their approximate spectral-spatial-temporal extent and effect size range. The channel-freq-time triplet corresponds to the sample yielding the upper bound of the effect size. *Abbreviations: BIP, biperiden; PLA, placebo; PRE: pre-drug; POST: post-drug; SCO, scopolamine.*

elicited by TMS, sensory processing, or both.

4.5. Limitations

One possible limitation of the present study is the choice of the sham procedure, which involved applying high-intensity ES in both *sham* and *active* TMS conditions. This approach deviates from previous studies, where ES is administered only in the *sham* TMS condition (Chowdhury et al., 2022; Rocchi et al., 2021). Our rationale was to closely approximate sensory-related EEG responses in both conditions by saturating sensory inputs with high-intensity ES. By subtracting *sham* from *active* TMS–EEG responses, we aimed to eliminate common sensory responses, thereby revealing the direct cortical activation elicited by TMS, as described in our previous study (Gordon et al., 2021). However, concerns arise regarding the use of high-intensity ES in the *active* TMS condition, as it may alter cortical responsiveness to TMS due to neurophysiological interactions. This raises doubts about the reliability of isolating genuine TMS–EEG responses through subtraction. Despite these concerns, we have reported that TEPs obtained through this sham procedure remained largely unchanged despite varying ES intensity used for saturation (Gordon et al., 2023a). Therefore, there is currently no evidence for a significant interaction between sensory responses and direct cortical responses from TMS measured by EEG. Additionally, using this sham procedure, we were able to successfully obtain distinct EEG responses with unique topographies that were likely due to direct cortical activation by TMS of specific brain regions, i.e., mPFC, AG, and SMA (Song et al., 2023).

Another limitation is the high inter-individual and inter-session variability of TEPs elicited with mPFC stimulation (Song et al., 2023), which may have hindered the discovery of modulation of TEPs by cholinergic transmission inhibition. The low signal-to-noise ratio may contribute to this variability, as suggested by the low amplitude of TEPs when applying TMS to the mPFC. While increasing TMS intensity may result in stronger direct cortical responses, as reported in a previous study (Kähkönen et al., 2005), it could also amplify unwanted signals, such as somatosensory and auditory EEG responses. Future studies may investigate strategies to optimize TMS–EEG measures in frontal regions while carefully controlling for TMS-associated sensory inputs.

Additionally, our study did not include the short-latency afferent inhibition (SAI) paradigm, which previous studies have linked to the central cholinergic system (Tremblay et al., 2019; Ziemann et al., 2015). While combining SAI with TMS–EEG has the potential to probe cholinergic neurotransmission in non-motor regions (Noda et al., 2016), the complexity of controlling for sensory contamination in the SAI TMS–EEG paradigm led us to focus on single-pulse TMS–EEG in this study. Lastly, while the order of TMS–EEG measurements targeting the mPFC, AG, and SMA was randomized, it was not fully counterbalanced across participants. Future studies should employ a fully counterbalanced design to minimize potential biases related to time-varying factors.

5. Conclusion

Our study demonstrates the involvement of mAChR-mediated cholinergic neurotransmission in TEPs but not in TIOs. Notably, this involvement is target-specific, as cholinergic inhibition through scopolamine, a non-selective mAChR antagonist, significantly increased the amplitude of a local TEP component between approximately 40 and 63 ms post-stimulus when TMS was applied to the SMA, but not to the mPFC or AG. The selective M1 mAChR antagonist biperiden tended to produce a similar effect as scopolamine, but this was less pronounced. Moreover, cholinergic inhibition also affected SEPs but, importantly, its effects on TEPs were independent of those on SEPs. These findings add to the understanding of neuromodulator-mediated transmission in TMS–EEG responses, supporting their potential use in further physiological and clinical research.

Ethical statement

The study was approved by the ethics committee of the medical faculty of Tübingen University (protocol number 638/2020BO1) and was conducted in accordance with the Declaration of Helsinki. Informed consent was obtained from all individual participants included in the study.

Funding

The study was funded by the European Research Council (ERC Synergy) under the European Union's Horizon 2020 research and innovation program (ConnectToBrain, grant number 810377).

Declaration of generative AI in scientific writing

During the preparation of this work, the first author used ChatGPT-4o (freely available at https://chatgpt.com/) solely for grammar correctness, word choice, and semantics improvement. After using this tool, the first author and all co-authors reviewed and edited the content as needed and take full responsibility for the content of the publication.

CRediT authorship contribution statement

Yufei Song: Conceptualization, Methodology, Formal analysis, Investigation, Data curation, Writing – original draft, Writing – review & editing, Visualization, Project administration. **Pedro C. Gordon:** Conceptualization, Methodology, Writing – review & editing, Supervision, Project administration. **Olivier Roy:** Methodology, Writing – review & editing, Visualization. **Johanna Metsomaa:** Software, Methodology, Writing – review & editing. **Paolo Belardinelli:** Software, Methodology, Writing – review & editing. **Maryam Rostami:** Software, Methodology, Writing – review & editing. **Ulf Ziemann:** Conceptualization, Methodology, Validation, Resources, Writing – review & editing, Supervision, Project administration, Funding acquisition.

Declaration of competing interest

The authors declare no conflicts of interest.

Data availability

The code used is available in GitHub: https://github.com/Song-Yufei/anti-cholinergic-drugs-on-TMS-EEG-responses. The preprocessed TMS–EEG data, individual head models and lead field matrices that support the findings of the manuscript are deposited in the repository FDAT: https://doi.org/10.57754/FDAT.d0ms3-z0v09 with access granted under specified conditions, i.e., EULA (End User License Agreement) signed by the user.

Appendix A. Supplementary data

Supplementary data to this article can be found online at https://doi.org/10.1016/j.pnpbp.2024.111167.

References

Abudukeyoumu, N., Hernandez-Flores, T., Garcia-Munoz, M., Arbuthnott, G.W., 2019. Cholinergic modulation of striatal microcircuits. Eur. J. Neurosci. 49, 604–622.
Andersen, L.M., Lundqvist, D., 2019. Somatosensory responses to nothing: an MEG study of expectations during omission of tactile stimulations. NeuroImage 184, 78–89.
Aosaki, T., Miura, M., Suzuki, T., Nishimura, K., Masuda, M., 2010. Acetylcholine–dopamine balance hypothesis in the striatum: an update. Geriatr Gerontol Int 10, S148–S157.
Arnold, H., Burk, J., Hodgson, E., Sarter, M., Bruno, J., 2002. Differential cortical acetylcholine release in rats performing a sustained attention task versus behavioral control tasks that do not explicitly tax attention. Neuroscience 114, 451–460.

Augustine, F., Singer, H.S., 2018. Merging the pathophysiology and pharmacotherapy of tics. Tremor Other Hyperkinet. Mov. 8.
Baakman, A.C., Alvarez-Jimenez, R., Rissmann, R., Klaassen, E.S., Stevens, J., Goulooze, S.C., den Burger, J.C., Swart, E.L., van Gerven, J.M., Groeneveld, G.J., 2017. An anti-nicotinic cognitive challenge model using mecamylamine in comparison with the anti-muscarinic cognitive challenge using scopolamine. Br. J. Clin. Pharmacol. 83, 1676–1687.
Baayen, R.H., Milin, P., 2010. Analyzing reaction times. Int. J. Psychol. Res. 3, 12–28.
Bakker, C., van Esdonk, M.J., Stuurman, R.F.E., Borghans, L.G., de Kam, M.L., van Gerven, J.M., Groeneveld, G.J., 2021. Biperiden challenge model in healthy elderly as proof-of-pharmacology tool: a randomized, placebo-controlled trial. J. Clin. Pharmacol. 61, 1466–1478.
Ballinger, E.C., Ananth, M., Talmage, D.A., Role, L.W., 2016. Basal forebrain cholinergic circuits and signaling in cognition and cognitive decline. Neuron 91, 1199–1218.
Balota, D.A., Aschenbrenner, A.J., Yap, M.J., 2013. Additive effects of word frequency and stimulus quality: the influence of trial history and data transformations. J. Exp. Psychol. Learn. Mem. Cogn. 39, 1563.
Bauer, M., Oostenveld, R., Peeters, M., Fries, P., 2006. Tactile spatial attention enhances gamma-band activity in somatosensory cortex and reduces low-frequency activity in parieto-occipital areas. J. Neurosci. 26, 490–501.
Belardinelli, P., König, F., Liang, C., Premoli, I., Desideri, D., Müller-Dahlhaus, F., Gordon, P.C., Zipser, C., Zrenner, C., Ziemann, U., 2021. TMS-EEG signatures of glutamatergic neurotransmission in human cortex. Sci. Rep. 11, 8159.
Bentley, P., Driver, J., Dolan, R.J., 2011. Cholinergic modulation of cognition: insights from human pharmacological functional neuroimaging. Prog. Neurobiol. 94, 360–388.
Biondi, A., Rocchi, L., Santoro, V., Rossini, P., Beatch, G., Richardson, M., Premoli, I., 2022. Spontaneous and TMS-related EEG changes as new biomarkers to measure anti-epileptic drug effects. Sci. Rep. 12, 1919.
Bohnen, N.I., Grothe, M.J., Ray, N.J., Müller, M.L., Teipel, S.J., 2018. Recent advances in cholinergic imaging and cognitive decline—revisiting the cholinergic hypothesis of dementia. Curr. Geriatr. Rep. 7, 1–11.
Boksem, M.A., Meijman, T.F., Lorist, M.M., 2005. Effects of mental fatigue on attention: an ERP study. Cogn. Brain Res. 25, 107–116.
Caldenhove, S., Borghans, L., Blokland, A., Sambeth, A., 2017. Role of acetylcholine and serotonin in novelty processing using an oddball paradigm. Behav. Brain Res. 331, 199–204.
Casarotto, S., Turco, F., Comanducci, A., Perretti, A., Marotta, G., Pezzoli, G., Rosanova, M., Isaias, I.U., 2019. Excitability of the supplementary motor area in Parkinson's disease depends on subcortical damage. Brain Stimul. 12, 152–160.
Cash, R.F.H., Noda, Y., Zomorrodi, R., Radhu, N., Farzan, F., Rajji, T.K., Fitzgerald, P.B., Chen, R., Daskalakis, Z.J., Blumberger, D.M., 2017. Characterization of glutamatergic and GABAA-mediated neurotransmission in motor and dorsolateral prefrontal cortex using paired-pulse TMS–EEG. Neuropsychopharmacology 42, 502–511. https://doi.org/10.1038/npp.2016.133.
Casula, E.P., Pellicciari, M.C., Picazio, S., Caltagirone, C., Koch, G., 2016. Spike-timing-dependent plasticity in the human dorso-lateral prefrontal cortex. Neuroimage 143, 204–213.
Chowdhury, N.S., Rogasch, N.C., Chiang, A.K., Millard, S.K., Skippen, P., Chang, W.-J., Bilska, K., Si, E., Seminowicz, D.A., Schabrun, S.M., 2022. The influence of sensory potentials on transcranial magnetic stimulation–electroencephalography recordings. Clin. Neurophysiol. 140, 98–109.
Cohen, M.X., 2014. Analyzing Neural Time Series Data: Theory and Practice. MIT press.
Colangelo, C., Shichkova, P., Keller, D., Markram, H., Ramaswamy, S., 2019. Cellular, synaptic and network effects of acetylcholine in the neocortex. Front. Neural Circuits 13, 24.
Conde, V., Tomasevic, L., Akopian, I., Stanek, K., Saturnino, G.B., Thielscher, A., Bergmann, T.O., Siebner, H.R., 2019. The non-transcranial TMS-evoked potential is an inherent source of ambiguity in TMS-EEG studies. Neuroimage 185, 300–312.
Curran, H., Pooviboonsuk, P., Dalton, J., Lader, M., 1998. Differentiating the effects of centrally acting drugs on arousal and memory: an event-related potential study of scopolamine, lorazepam and diphenhydramine. Psychopharmacology 135, 27–36.
Darmani, G., Zipser, C.M., Böhmer, G.M., Deschet, K., Müller-Dahlhaus, F., Belardinelli, P., Schwab, M., Ziemann, U., 2016. Effects of the selective α5-GABAAR antagonist S44819 on excitability in the human brain: a TMS–EMG and TMS–EEG phase I study. J. Neurosci. 36, 12312–12320.
Delorme, A., Makeig, S., 2004. EEGLAB: an open source toolbox for analysis of single-trial EEG dynamics including independent component analysis. J. Neurosci. Methods 134, 9–21.
Doyle Gaynor, L., Kühn, A., Dileone, M., Litvak, V., Eusebio, A., Pogosyan, A., Androulidakis, A., Tisch, S., Limousin, P., Insola, A., others, 2008. Suppression of beta oscillations in the subthalamic nucleus following cortical stimulation in humans. Eur. J. Neurosci. 28, 1686–1695.
Fernandez, L., Biabani, M., Do, M., Opie, G.M., Hill, A.T., Barham, M.P., Teo, W.-P., Byrne, L.K., Rogasch, N.C., Enticott, P.G., 2021. Assessing cerebellar-cortical connectivity using concurrent TMS-EEG: a feasibility study. J. Neurophysiol. 125, 1768–1787.
Fields, E.C., Kuperberg, G.R., 2020. Having your cake and eating it too: flexibility and power with mass univariate statistics for ERP data. Psychophysiology 57, e13468.
Gordon, P.C., Jovellar, D.B., Song, Y., Zrenner, C., Belardinelli, P., Siebner, H.R., Ziemann, U., 2021. Recording brain responses to TMS of primary motor cortex by EEG–utility of an optimized sham procedure. Neuroimage 245, 118708.
Gordon, P.C., Song, Y., Jovellar, B., Belardinelli, P., Ziemann, U., 2023a. No evidence for interaction between TMS-EEG responses and sensory inputs. Brain Stimul. 16, 25–27.
Gordon, P.C., Song, Y.F., Jovellar, D.B., Rostami, M., Belardinelli, P., Ziemann, U., 2023b. Untangling TMS-EEG responses caused by TMS versus sensory input using optimized sham control and GABAergic challenge. J. Physiol. 601, 1981–1998.
Grandchamp, R., Delorme, A., 2011. Single-trial normalization for event-related spectral decomposition reduces sensitivity to noisy trials. Front. Psychol. 2, 236.
Groppa, S., Oliviero, A., Eisen, A., Quartarone, A., Cohen, L., Mall, V., Kaelin-Lang, A., Mima, T., Rossi, S., Thickbroom, G., others, 2012. A practical guide to diagnostic transcranial magnetic stimulation: report of an IFCN committee. Clin. Neurophysiol. 123, 858–882.
Hernandez-Pavon, J.C., Veniero, D., Bergmann, T.O., Belardinelli, P., Bortoletto, M., Casarotto, S., Casula, E.P., Farzan, F., Fecchio, M., Julkunen, P., others, 2023. TMS combined with EEG: recommendations and open issues for data collection and analysis. Brain Stimul. 16, 567–593.
Himmelheber, A.M., Sarter, M., Bruno, J.P., 1997. Operant performance and cortical acetylcholine release: role of response rate, reward density, and non-contingent stimuli. Cogn. Brain Res. 6, 23–36.
Hui, J., Zomorrodi, R., Lioumis, P., Salavati, B., Rajji, T.K., Chen, R., Blumberger, D.M., Daskalakis, Z.J., 2020. Pharmacological mechanisms of interhemispheric signal propagation: a TMS-EEG study. Neuropsychopharmacology 45, 932–939. https://doi.org/10.1038/s41386-019-0468-7.
Ilmoniemi, R.J., Virtanen, J., Ruohonen, J., Karhu, J., Aronen, H.J., Näätänen, R., Katila, T., 1997. Neuronal responses to magnetic stimulation reveal cortical reactivity and connectivity. Neuroreport 8, 3537–3540.
Jackson, A.F., Bolger, D.J., 2014. The neurophysiological bases of EEG and EEG measurement: a review for the rest of us. Psychophysiology 51, 1061–1071.
Kähkönen, S., Komssi, S., Wilenius, J., Ilmoniemi, R.J., 2005. Prefrontal transcranial magnetic stimulation produces intensity-dependent EEG responses in humans. Neuroimage 24, 955–960.
Karamacoska, D., Barry, R.J., Steiner, G.Z., 2018. Electrophysiological underpinnings of response variability in the Go/NoGo task. Int. J. Psychophysiol. 134, 159–167.
Kim, J.-H., Jung, A.-H., Jeong, D., Choi, I., Kim, K., Shin, S., Kim, S.J., Lee, S.-H., 2016. Selectivity of neuromodulatory projections from the basal forebrain and locus ceruleus to primary sensory cortices. J. Neurosci. 36, 5314–5327.
Klinkenberg, I., Blokland, A., 2010. The validity of scopolamine as a pharmacological model for cognitive impairment: a review of animal behavioral studies. Neurosci. Biobehav. Rev. 34, 1307–1350.
Klinkenberg, I., Sambeth, A., Blokland, A., 2011. Acetylcholine and attention. Behav. Brain Res. 221, 430–442.
Kunnath, A.J., Gifford, R.H., Wallace, M.T., 2023. Cholinergic modulation of sensory perception and plasticity. Neurosci. Biobehav. Rev. 152, 105323.
Kuriakose, R., Saha, U., Castillo, G., Udupa, K., Ni, Z., Gunraj, C., Mazzella, F., Hamani, C., Lang, A.E., Moro, E., others, 2010. The nature and time course of cortical activation following subthalamic stimulation in Parkinson's disease. Cereb. Cortex 20, 1926–1936.
Lawrence, N.S., Ross, T.J., Stein, E.A., 2002. Cognitive mechanisms of nicotine on visual attention. Neuron 36, 539–548.
Maris, E., Oostenveld, R., 2007. Nonparametric statistical testing of EEG-and MEG-data. J. Neurosci. Methods 164, 177–190.
Massimini, M., Ferrarelli, F., Huber, R., Esser, S.K., Singh, H., Tononi, G., 2005. Breakdown of cortical effective connectivity during sleep. Science 309, 2228–2232.
Maurice, N., Liberge, M., Jaouen, F., Ztaou, S., Hanini, M., Camon, J., Deisseroth, K., Amalric, M., Kerkerian-Le Goff, L., Beurrier, C., 2015. Striatal cholinergic interneurons control motor behavior and basal ganglia function in experimental parkinsonism. Cell Rep. 13, 657–666.
Metsomaa, J., Song, Y., Mutanen, T.P., Gordon, P.C., Ziemann, U., Zrenner, C., Hernandez-Pavon, J.C., 2024. Adapted beamforming: a robust and flexible approach for removing various types of artifacts from TMS–EEG data. Brain Topogr. 1–25.
Meyer, M., Lamers, D., Kayhan, E., Hunnius, S., Oostenveld, R., 2021. Enhancing reproducibility in developmental EEG research: BIDS, cluster-based permutation tests, and effect sizes. Dev. Cogn. Neurosci. 52, 101036.
Muñoz, W., Rudy, B., 2014. Spatiotemporal specificity in cholinergic control of neocortical function. Curr. Opin. Neurobiol. 26, 149–160.
Nadim, F., Bucher, D., 2014. Neuromodulation of neurons and synapses. Curr. Opin. Neurobiol. 29, 48–56.
Nakano, K., Kayahara, T., Tsutsumi, T., Ushiro, H., 2000. Neural circuits and functional organization of the striatum. J. Neurol. 247, V1–V15.
Ni, Z., Kim, S.J., Phielipp, N., Ghosh, S., Udupa, K., Gunraj, C.A., Saha, U., Hodaie, M., Kalia, S.K., Lozano, A.M., others, 2018. Pallidal deep brain stimulation modulates cortical excitability and plasticity. Ann. Neurol. 83, 352–362.
Noda, Y., Cash, R.F.H., Zomorrodi, R., Dominguez, L.G., Farzan, F., Rajji, T.K., Barr, M.S., Chen, R., Daskalakis, Z.J., Blumberger, D.M., 2016. A combined TMS-EEG study of short-latency afferent inhibition in the motor and dorsolateral prefrontal cortex. J. Neurophysiol. 116, 938–948. https://doi.org/10.1152/jn.00260.2016.
Novembre, G., Pawar, V.M., Kilintari, M., Bufacchi, R.J., Guo, Y., Rothwell, J.C., Iannetti, G.D., 2019. The effect of salient stimuli on neural oscillations, isometric force, and their coupling. NeuroImage 198, 221–230.
Oostenveld, R., Fries, P., Maris, E., Schoffelen, J.-M., 2011. FieldTrip: open source software for advanced analysis of MEG, EEG, and invasive electrophysiological data. Comput. Intell. Neurosci. 2011, 1–9.
Parikh, V., Kozak, R., Martinez, V., Sarter, M., 2007. Prefrontal acetylcholine release controls cue detection on multiple timescales. Neuron 56, 141–154.
Pellicciari, M.C., Veniero, D., Miniussi, C., 2017. Characterizing the cortical oscillatory response to TMS pulse. Front. Cell. Neurosci. 11, 38.
Picciotto, M.R., Higley, M.J., Mineur, Y.S., 2012. Acetylcholine as a neuromodulator: cholinergic signaling shapes nervous system function and behavior. Neuron 76, 116–129.

Pinto, L., Goard, M.J., Estandian, D., Xu, M., Kwan, A.C., Lee, S.-H., Harrison, T.C., Feng, G., Dan, Y., 2013. Fast modulation of visual perception by basal forebrain cholinergic neurons. Nat. Neurosci. 16, 1857–1863.
Premoli, I., Castellanos, N., Rivolta, D., Belardinelli, P., Bajo, R., Zipser, C., Espenhahn, S., Heidegger, T., Müller-Dahlhaus, F., Ziemann, U., 2014. TMS-EEG signatures of GABAergic neurotransmission in the human cortex. J. Neurosci. 34, 5603–5612.
Premoli, I., Bergmann, T.O., Fecchio, M., Rosanova, M., Biondi, A., Belardinelli, P., Ziemann, U., 2017. The impact of GABAergic drugs on TMS-induced brain oscillations in human motor cortex. Neuroimage 163, 1–12.
Rocchi, L., Di Santo, A., Brown, K., Ibáñez, J., Casula, E., Rawji, V., Di Lazzaro, V., Koch, G., Rothwell, J., 2021. Disentangling EEG responses to TMS due to cortical and peripheral activations. Brain Stimul. 14, 4–18.
Rosanova, M., Casali, A., Bellina, V., Resta, F., Mariotti, M., Massimini, M., 2009. Natural frequencies of human corticothalamic circuits. J. Neurosci. 29, 7679–7685.
Salavati, B., Rajji, T.K., Zomorrodi, R., Blumberger, D.M., Chen, R., Pollock, B.G., Daskalakis, Z.J., 2018. Pharmacological manipulation of cortical inhibition in the dorsolateral prefrontal cortex. Neuropsychopharmacology 43, 354–361. https://doi.org/10.1038/npp.2017.104.
Sassenhagen, J., Draschkow, D., 2019. Cluster-based permutation tests of MEG/EEG data do not establish significance of effect latency or location. Psychophysiology 56, e13335.
Sawilowsky, S.S., 2009. New effect size rules of thumb. J. Mod. Appl. Stat. Methods 8, 26.
Siebner, H.R., Funke, K., Aberra, A.S., Antal, A., Bestmann, S., Chen, R., Classen, J., Davare, M., Di Lazzaro, V., Fox, P.T., others, 2022. Transcranial magnetic stimulation of the brain: what is stimulated?–a consensus and critical position paper. Clin. Neurophysiol. 140, 59–97.
Song, Y., Gordon, P.C., Metsomaa, J., Rostami, M., Belardinelli, P., Ziemann, U., 2023. Evoked EEG responses to TMS targeting regions outside the primary motor cortex and their test–retest reliability. Brain Topogr. 1–18.
Stein, E.A., Pankiewicz, J., Harsch, H.H., Cho, J.-K., Fuller, S.A., Hoffmann, R.G., Hawkins, M., Rao, S.M., Bandettini, P.A., Bloom, A.S., 1998. Nicotine-induced limbic cortical activation in the human brain: a functional MRI study. Am. J. Psychiatry 155, 1009–1015.
Strafella, A.P., Vanderwerf, Y., Sadikot, A.F., 2004. Transcranial magnetic stimulation of the human motor cortex influences the neuronal activity of subthalamic nucleus. Eur. J. Neurosci. 20, 2245–2249.
Tabachnick, B.G., Fidell, L.S., 2007. Experimental Designs Using ANOVA. Thomson/Brooks/Cole Belmont, CA.
Thiele, A., 2013. Muscarinic signaling in the brain. Annu. Rev. Neurosci. 36, 271–294.
Thienel, R., Kellermann, T., Schall, U., Voss, B., Reske, M., Halfter, S., Sheldrick, A.J., Radenbach, K., Habel, U., Shah, N.J., others, 2009. Muscarinic antagonist effects on executive control of attention. Int. J. Neuropsychopharmacol. 12, 1307–1317.
Tremblay, S., Rogasch, N.C., Premoli, I., Blumberger, D.M., Casarotto, S., Chen, R., Di Lazzaro, V., Farzan, F., Ferrarelli, F., Fitzgerald, P.B., others, 2019. Clinical utility and prospective of TMS–EEG. Clin. Neurophysiol. 130, 802–844.
Tsuboi, D., Nagai, T., Yoshimoto, J., Kaibuchi, K., 2024. Neuromodulator regulation and emotions: insights from the crosstalk of cell signaling. Front. Mol. Neurosci. 17, 1376762.
Utter, A.A., Basso, M.A., 2008. The basal ganglia: an overview of circuits and function. Neurosci. Biobehav. Rev. 32, 333–342.
Walker, H.C., Huang, H., Gonzalez, C.L., Bryant, J.E., Killen, J., Cutter, G.R., Knowlton, R.C., Montgomery, E.B., Guthrie, B.L., Watts, R.L., 2012. Short latency activation of cortex during clinically effective subthalamic deep brain stimulation for Parkinson's disease. Mov. Disord. 27, 864–873.
Záborszky, L., Gombkoto, P., Varsanyi, P., Gielow, M.R., Poe, G., Role, L.W., Ananth, M., Rajebhosale, P., Talmage, D.A., Hasselmo, M.E., others, 2018. Specific basal forebrain–cortical cholinergic circuits coordinate cognitive operations. J. Neurosci. 38, 9446–9458.
Ziemann, U., Reis, J., Schwenkreis, P., Rosanova, M., Strafella, A., Badawy, R., Müller-Dahlhaus, F., 2015. TMS and drugs revisited 2014. Clin. Neurophysiol. 126, 1847–1868.
Ztaou, S., Amalric, M., 2019. Contribution of cholinergic interneurons to striatal pathophysiology in Parkinson's disease. Neurochem. Int. 126, 1–10.